# Immunogenicity and Structural Features of a Stabilized Clade-C HIV-1 Env Derived from a Pediatric Elite-neutralizer

Swarandeep Singh[1,†], Sanjeev Kumar[1,2,†], Arnab Chatterjee[3,†], Lakshay Malhotra[4], Abdul Rahman[1], Ifrah Andrabi[1], Bapan Mondal[3], Sanket Katpara[1], Shaifali Sharma[1], Harsh Bhakri[1], Anjli Gaur[1] ,Tanu Bansal[1], Muneeb Pervez[1], Vikram Iyer[1] , Abdul Wahid Hussain[1], Shubbir Ahmed[6], Rajesh Kumar[5], Ethayathulla Abdul Samath[4], Rakesh Lodha[7], Somnath Dutta[3*], Kalpana Luthra[1*]

[1]Department of Biochemistry, All India Institute of Medical Sciences, New Delhi, India
[2]ICGEB-Emory Vaccine Center, International Center for Genetic Engineering and Biotechnology, New Delhi, India
[3]Molecular Biophysics Unit, Indian Institute of Science, Bangalore, India
[4]Department of Biophysics, All India Institute of Medical Sciences, New Delhi, India
[5]Indian Institute of Technology, Roorkee, India
[6] Centralized Core Research Facility, All India Institute of Medical Sciences, New Delhi, India
[7] Department of Pediatrics, All India Institute of Medical Sciences, New Delhi, India

[†]These authors contributed equally
[*]Correspondence**:** somnath@iisc.ac.in (S.D.), kalpanaluthra@gmail.com (K.L.)

**Keywords:** HIV-1 vaccine, Immunogenicity**,** Neutralizing Antibodies, Cryo-EM structure

## ABSTRACT

The envelope (Env) glycoprotein from viruses circulating in elite-neutralizers-individuals who naturally develop broadly neutralizing antibody (bNAb) responses, serves as potential template for rational HIV-1 vaccine design. Here, we engineered a soluble clade-C Env trimer (330) derived from a pediatric elite-neutralizer (AIIMS_330) using SOSIP, NFL, and self-assembling ferritin-nanoparticles (NP) platforms. Both Env SOSIP and NP-displayed Envs exhibited high thermostability and nanomolar binding affinity to diverse HIV-1 bNAbs, with minimal reactivity to non-neutralizing antibodies, indicative of a native-like antigenic profile. A cryo-EM structure of the 330-SOSIP trimer in complex with the autologous bNAb 44m, revealed recognition of the GDIR motif and N332 supersite with additional contacts at T144, and T413. Rabbits immunized with the SOSIP and NP elicited potent autologous and other tier-1 clade-C viruses neutralizing

31 responses, supporting the utility of multivalent vaccine. These findings broadens our
32 understanding of the structure and immunogenicity of the HIV-1 Env from pediatric ENs and
33 contributes valuable information towards a rational immunogen design.

34

35 **INTRODUCTION**

36 A critical goal in HIV vaccine development is to elicit broadly neutralizing antibodies
37 (bNAbs) in uninfected and high-risk individuals[1]. Elite neutralizers (ENs), a rare group of HIV-1-
38 infected individuals who develop exceptionally potent bNAb responses, provide valuable
39 blueprints for rational HIV-1 immunogen design, aimed at inducing similar bNAb responses
40 upon vaccination[1–3]. Studies involving simian-human immunodeficiency virus (SHIV) challenges
41 in nonhuman primates (NHPs) have indicated that passive immunization with bNAbs can
42 effectively prevent infection, supporting the development of an HIV-1 vaccine that induces such
43 protective immune responses in humans upon vaccination[4–8]. Stabilized HIV-1 envelope (Env)
44 glycoproteins have emerged as promising candidates for immunogen design, with the potential
45 to elicit protective immune responses through vaccination, based on insights from the RV144
46 Thai trial[9,10]. Native like HIV-1 Env trimers, particularly the clade-A BG505 Env have shown the
47 ability to induce neutralizing antibody (nAb) responses in animal models and are currently
48 under evaluation in clinical trials[11–18]. HIV-1 clade C, predominates global HIV-1 infection with
49 more than 50% infections[19,20]. A limited number of clade-C Envs has been stabilized; with low
50 expression levels and instability, posing hurdles to develop clade C Env-based vaccines[21–24].

51 Recent investigations highlight distinct differences in surface antigen presentation
52 between HIV-1 and HPV, contributing to HIV-1's limited ability to elicit a strong immune
53 response compared to HPV[25]. In contrast, currently approved multivalent vaccines for HPV and
54 HBV generate robust immune responses with >95% efficacy[26–28]. Recent studies suggest that
55 single Env-based vaccine regimens may not be the most effective approach for HIV-1 prevention.
56 Notably, presenting HIV-1 Env trimers on self-assembling ferritin nanoparticles has shown
57 promise in eliciting robust immune response in rabbits, suggesting improved
58 immunogenicity[29,30]. Studies also suggest that HIV-infected children who often acquire the
59 infection through vertical transmission, are inherently better at generating bNAbs than adults[31–
60 36]. The relative immaturity of the immune system in children may allow for more effective

61 protective immune responses, as founder virus encounters minimal selection pressure,
62 providing the evolving B-cells an advantage in generating NAbs that effectively neutralize
63 contemporary viruses[31–33,37]. Env trimers from contemporaneous viruses can serve as effective
64 tools for immunogen design, and structural characterization of Env in complex with autologous
65 bNAbs from the same donor can provide valuable insights for vaccine development[36].

66 We previously reported on a pair of HIV-1-infected monozygotic twins (AIIMS_330 and
67 AIIMS_329) demonstrating elite neutralizing activity, with longitudinal sampling of AIIMS_330
68 revealing sustained elite neutralizing activity. The Env from this EN exhibited multiple broad
69 bNAb epitope specificities, making it an ideal template for designing and characterizing HIV-1
70 Env mimics[33,35]. In this study, we designed and characterized an HIV-1 Clade-C 330 Env trimer
71 derived from a pediatric EN AIIMS_330, as soluble SOSIP & NFL Env trimers, alongside tailoring
72 the Env to display a repetitive array of HIV-1 trimers on self-assembling ferritin nanoparticles
73 (NPs)[11,29,38]. Designed Env constructs, stabilized by trimer-stabilizing mutations, exhibited
74 enhanced expression and a greater propensity to assemble into native-like HIV-1 Env
75 mimics[12,15,39,40]. The 330 Env constructs exposed multiple epitopes and demonstrated strong
76 affinity to bNAbs while occluding the immunodominant epitopes of non-neutralizing antibodies
77 (non-NAbs). Ferritin NPs exhibited strong immunogenicity and tier-1 autologous neutralizing
78 activity, upon immunization in rabbits compared to soluble counterparts. Negative stain-
79 electron microscopy (NS-EM) showed that both soluble Envs and multivalent NP adopted native-
80 like morphology. A cryo-EM structure, revealed a stable, well-organized Envelope structure in
81 the prefusion closed conformation of the 330 SOSIP Env trimer. Structural insights from the
82 cryo-EM model of the 330 SOSIP Env trimer in complex with the autologous bNAb 44m, a V3-
83 glycan-specific potent bNAb identified from the AIIMS_330 EN[36], provide information on the
84 antigenic determinants. Collectively, this study broadens our understanding of the structure and
85 immunogenicity of the HIV-1 Env from pediatric ENs. The 330 Env could serve as valuable
86 antigenic probes for HIV-1 bNAb discovery and potential Env for a multivalent vaccine design
87 and vaccination strategies.

88

89

90

91 **RESULTS**

92 **Design & biophysical characterization of 330 Env trimers and ferritin nanoparticles**

93 Previously we reported a pair of HIV-1 chronically infected monozygotic twins AIIMS_330
94 & AIIMS_329 exhibiting elite plasma neutralizing activity[35]. Over five years of longitudinal
95 sampling, the AIIMS_330 EN showed sustained evolution of plasma bNAbs targeting major
96 neutralizing determinants on the HIV-1 Env glycoprotein[33,35,41]. The pseudoviral Env clone
97 330.16.E6, derived from the AIIMS_330 EN, exhibited high susceptibility to neutralization by a
98 broad range of HIV-1 bNAbs with multiple epitope specificity, along with autologous
99 contemporaneous plasma antibodies, and resistance to the panel of non-nAbs tested[33,35].
100 Therefore, we engineered this Env in membrane soluble forms, as SOSIP.664 gp120-gp41
101 cleaved Env trimers, NFL.664 gp140 single-chain uncleaved Env trimers and SOSIP Env trimers
102 on self-assembling ferritin NPs to achieve multivalency (Figure 1 A-C). The 330 Env trimers were
103 stabilized by incorporating mutations for increased expression and trimerization, as illustrated
104 in Figure 1A-D, Table S1. The SOSIP Env was designed by introducing a SOS disulfide bond
105 (A501C-T605C)[46], an I559P mutation[42], and an optimized furin cleavage site (RRRRRR)[47] . We
106 designed the NFL Env construct, that carried the I559P mutation, by linking the gp120 and gp41
107 using a flexible glycine-serine linker (GGGGSGGGGS)[38]. Both Env constructs were human codon-
108 optimized to enhance expression in mammalian systems.

109 The stabilized and optimized 330 Envs were expressed in HEK293F cells, followed by a
110 two-step purification viz. HIV-1 Env trimer specific bNAb PGT145-Immunoaffinity
111 chromatography followed by Size Exclusion Chromatography (SEC). The SEC purification of 330
112 Env trimers (SOSIP and NFL) yielded a peak at an elution volume of 10 mL, which shifted further
113 upward for ferritin nanoparticles, eluting at 8.5 mL on a Superdex 200 10/300 column (Figure
114 1E). The purification yield of 330 Env trimers following SEC was around ~1 mg/L for SOSIP and
115 ~1.45 mg/L for NFL (Figure S2), which was higher or comparable to the Indian and South
116 African Clade-C strains (CZA97: ~0.4-0.6 mg/mL, 329 SOSIP: ~0.6 mg/mL, 16055 NFL: ~2
117 mg/mL)[23,48–50]. The NFL trimer of Env 330 had better expression yields than the SOSIP version,
118 likely due to the increased stability and functionality provided by the covalent linkage between
119 the gp120 and gp41 subunits, resulting in more functional gp140 molecules[38,50]. However, low
120 yield of Ferritin NPs was observed, around 0.05 mg/L, likely due to the complex assembly of Env
121 trimers into synthesized ferritin nanocages as reported previously[51,52]. The 330 Env trimers

122 displayed single band on Blue Native-PAGE (BN-PAGE) stained with Coomassie, whereas the 330
123 ferritin NPs were too large to efficiently enter the gels and visible at the top of the lanes,
124 indicating the high purity of Env trimers and NPs preparations (Figure S2-Left). The SDS-PAGE
125 analysis revealed intact trimeric nature of the 330 Env proteins under non-reducing conditions
126 that separated as monomers in the presence of DTT under reducing conditions (Figure S2-
127 Right). Negative-Stain Electron Microscopy (NS-EM) reference-free two-dimensional (2D) class
128 averages demonstrated that over 99% of the gp140 proteins adopted a native-like trimeric
129 morphology, with multiple copies of the Env spikes efficiently displayed on the self-assembling
130 ferritin NPs (Figure 1F, Supplementary S3). The 3D model of soluble gp140 trimers reveals a
131 trilobular structure, while ferritin NPs display multiple copies of Env spikes (Figure 1G).
132 Thermal stability & secondary structures of 330 Envs were evaluated using sypro-orange
133 Differential Scanning Fluorimetry (DSF) and by Circular Dichroism (CD) spectroscopy. The 330
134 SOSIP Env exhibited a Tm of ~74°C indicating its ability to retain its structural integrity even at
135 elevated temperatures (Figure 1H, S4 A-B). The CD spectra of 330 SOSIP Env reveal ~25% alpha-
136 helical and ~25% antiparallel beta-sheet content, contributing to the stability and rigidity of the
137 Env, while random coils impart the flexibility required for molecular recognition, collectively
138 suggesting a thermodynamically stable secondary structure for the Envelope protein (Figure S4
139 C-D). Overall, biophysical characterization demonstrated that the 330 Envs are well-stabilized,
140 and effectively displayed on ferritin NP cages.

141 **Antigenicity of 330 Env trimers and ferritin nanoparticles indicated strong binding**
142 **affinity to HIV-1 bNAbs**

143 Next, we assessed the antigenicity of the 330 Envs using binding ELISA with an extensive
144 panel of HIV-1 bNAbs and non-nAbs. The 330 Env trimers exhibited well-exposed epitopes
145 recognized by potent bNAbs, including the V1V2 apex (PGT145, PGDM1400, CAP256.25), the V3-
146 glycan supersite (2G12, PGT121, 10-1074, AIIMS-P01), the CD4 binding site (VRC01, N6), and
147 the gp120-gp41 interface (PGT151), while showing minimal reactivity to non-NAbs (F105, A32,
148 48d, 17b+sCD4), suggesting that the 330 Env trimers adopt native-like conformations (Figure 2).
149 The antigenic profile of ferritin NPs was found to resemble that of SOSIP, though with less
150 saturation to tested monoclonal antibodies (mAbs) concentration and allowing all the
151 conformational epitopes to be accessible to HIV-1 neutralizing mAbs targeting to the Envs
152 presented on the nanoparticle. A minor degree of binding of the non-NAbs was observed with

153 NFL and ferritin particles, with negligible to SOSIP. Notably, the 330 Env trimers and particles
154 exhibited preferential affinity for neutralizing mAbs over non-neutralizing mAbs.

155 Subsequently, we assessed the binding affinity of 330 Envs to neutralizing & non-
156 neutralizing mAbs with distinct specificities was then assessed by BLI-Octet analysis. To assess
157 binding affinity and kinetics, we selected conformation-specific bNAbs (PGT145, PGDM1400, and
158 PGT151) as well as non-neutralizing antibodies (F105, 17b, and sCD4). The gp140 Envs (affinity)
159 & ferritin NPs (avidity) exhibited strong binding affinity to the tested bNAbs (Figure 3). The
160 SOSIP variants (Ferritin NPs) (KD 1.07 nm) & NFL (KD 1.39 nm) showed a high affinity of ~1nM
161 to the V1V2 directed bNAb PGT145. A similar trend in binding of PGDM1400 with SOSIP (KD
162 1.34 nm) & NFL Env (KD 3.32 nm) was observed respectively. The interface-directed bNAb
163 PGT151 demonstrated an exceptionally high affinity to SOSIP variants (Ferritin NPs), with an
164 affinity of ~5 pM, indicating that the PGT151 epitopes on the Env proteins displayed on the
165 nanoparticle were highly accessible (Table S2). We observed that PGT145-purified SOSIP
166 trimers were efficiently cleaved at the gp120-gp41 junction, as indicated by strong binding to the
167 cleavage-specific bNAb PGT151, while no binding was detected with NFL trimer (Figure 2 & 3).
168 The introduction of intraprotomer locking 201C –433C disulfide bond as described previously[50],
169 in these constructs prevented the CD4-induced Env rearrangements as assessed by low
170 reactivity with sCD4 & 17b non-nAbs, indicating the prefusion conformation of the Envelopes. As
171 expected, and consistent with the ELISA binding results, the 330 Envs exhibited minimal
172 reactivity to the non-NAbs F105 and 17b+sCD4 (Figure 2 & 3, Table S2). Collectively, these
173 findings suggest that both the soluble Envs and multivalent NPs adopt a native-like
174 conformation, exposing multiple key bNAb epitopes while shielding the immunodominant
175 epitopes targeted by non-NAbs. Based on the negligible antigenic reactivity of the SOSIP Env
176 with non-nAbs, we next performed the structural analysis of the SOSIP Env.

177 **Cryo-EM structure of 330 SOSIP Env in complex with autologous bNAb 44m**

178 The structure of the natively glycosylated 330 SOSIP Env was solved using single-particle
179 cryo-electron microscopy (cryo-EM). A total 109004 number of particles were analyzed to
180 determine the 2D class averages and reconstruct the trilobular 3D model of 330 SOSIP Env in its
181 prefusion closed conformations (Figure S5 A-C). In a recent study, we reported heavy chain
182 matured HIV-1 lineage bNAb 44m, which effectively neutralizes its autologous pseudovirus,
183 330.16.E6, from which the 330 Env trimer is derived[36]. We aimed to investigate the key

interacting residues of bNAb 44m to its autologous Envelope 330. A cryo-EM structure of 330 SOSIP Env in complex with 44m bNAb was solved (Figure 5, S6). The architecture of 330 Env displayed the trilobular shapes of trimers with three extra densities of corresponding bNAb 44m Fab bound moieties (Figure 5 A-B, Supply S6A). The model showed that three 44m FAbs bind to each gp120 monomeric subunit, enabling effective neutralization (Figure 5C-F). The interacting surface area covered by the mainly by heavy chain of 44m and 330 Envs are 522 $Å^2$, and 554 $Å^2$ respectively (Figure 5B). The model further reveals that the 44m CDRH1 is positioned near the 330 Env V1V2 loop, while CDRH2 and CDRH3 are located near the V3 region (Figure 5C). Herein , we observed that 44m bNAb showed dependence on V3-glycan N332-supersite and GDIR motif along with distinct key residues identified in case of autologous Env 330 as compared to the heterologous clade-A Env BG505 as reported previously[36]. The key interacting residues include H31 in the CDRH1 loop, which forms a contact site with T144 in the V1 loop; Y52 and Y53 in the CDRH2 loop, which interact with D325 of the GDIR motif in the V3 region; R109 in the CDRH3 loop, which engages with glycan N332 in the V3 region; and T413 in the V4 loop of gp120 (Figure 5D). These interactions are primarily stabilized through hydrogen bonding and van der Waals forces. The glycan interaction at the 330 Env-44m Fab junction involves N146 from the V1 loop and N301 and N332 from the V3 loop (Figure 5E). The D235 residue was shielded within the hydrophobic cleft formed by the V3 loop of the gp120 region (Figure 5F). Next, we performed rigid-body docking of the 44m-BG505 atomic model (EMDB-36815) into our cryo-EM map (Figure S7). This analysis allowed us to investigate the binding modes of 44m[36] and other V3-glycan specific bNAbs 10-1074[53], PGT121[54], 438-B11[55], BG18[56], mature BG18[57], DH270.6[58], and BF520.1[59] to a 330 Env superimposed BG505 model. Our findings suggest that 44m interacts with the V3 loop via a slightly declining shift, similar to BF520 and BG18, but exhibits a distinct binding mode compared to PGT121 and 35022 (Figure S7).

**Structural and glycan homology of 330 Env to BG505**

To assess structural similarity, The HIV-1 Clade C 330 SOSIP trimer was superimposed onto a clade C Env 16055 NFL[60] (PDB: 5UM8) and a Clade-A Env BG505 SOSIP[61] (PDB: 4TVP). We observed that the 330 Env trimer exhibited greater structural similarity to BG505 Env, with lower root-mean-square deviations (RMSDs) of 0.685 Å for gp120 and 0.478 Å for gp41 compared to modelled 16055 Env, which had RMSDs of 0.798 Å for gp120 and 0.739 Å for gp41 (Figure 4A-D). Upon glycan prediction analysis by Los Alamos HIV-1 sequence database (LANGT), we observed that 330 Env lacked conserved PNGS at positions 295 and 339 in the

216 V3/C4 region and at position 130 in the V1V2 apex, in contrast to BG505 Env, which lacks PNGS
217 at positions 241 and 289 (Figure 4E). Since BG505-mediated immune responses are directed
218 against positions 241 and 289 in the V3 loop[62–64], the glycan hole in the V1V2 and V3/C4 region
219 of the 330 Env may favor the elicitation of immune responses focused on these regions. Next, we
220 calculated the total glycan hole area in the 330 Env using Los Alamos glycan shield mapping tool
221 (LAGSM), suggesting that the optimal protein accessible area was 967 $Å^2$, compared to BG505,
222 B41, C9Z7A & Du422 counterparts (Figure 4F). The potential N-glycosylation sites (PNGS)
223 conserved in the 330 Env were determined by Los Alamos HIV-1 sequence database (LANGT)
224 using N-Glycosite tool. Conserved PNGS analysis revealed that 330 Env comprises of 28 PNGS
225 comparable to that reported in the BG505[65]& 16055[66] Envs (Figure 4F, Table S3). Targeting
226 exposed protein surfaces within glycan holes can be an effective strategy to boost the immune
227 response against these vulnerable sites. Overall, our structural homology modelling and glycan
228 analysis demonstrate that the stabilized clade-C Env 330 shares numerous features with the
229 well-studied BG505 Env, suggesting its capacity to adopt well-ordered structures.

230 **330 Ferritin nanoparticles and SOSIP trimer exhibit enhanced immunogenicity compared**
231 **to NFL in rabbits**

232 Following the establishment of native-like prefusion-closed Env structures, we next
233 evaluated and compared the immunogenicity of 330 Env trimers (SOSIP & NFL) and multivalent
234 ferritin NPs in New Zealand White (NZW) rabbits. Four groups of female rabbits were
235 immunized, primed at week 0, and boosted at weeks 4 and 20 and administered a dose of 20 μg
236 of 330 gp140 Env trimers or an equimolar amount (25 μg) of ferritin nanoparticles, formulated
237 with AddaVax™ adjuvant (Figure 6A). The AddaVax™ adjuvant is a squalene-based oil-in-water
238 nano-emulsion and has been shown not to impact the structural integrity or antigenicity of the
239 Env trimers, as demonstrated in previous studies[67,68]. Rabbits were bled at weeks 0, 4, 6, 16, 20,
240 and 22 and sera samples were subsequently evaluated for binding reactivity with the Env trimer
241 using capture ELISA and for neutralizing activity against Env pseudotyped viruses. First, we
242 evaluated the binding titers of the collected immune sera from different timepoints against the
243 immunogens tested and measured as median titers across each group. The binding titers of
244 immune sera exhibited a significant increase between 4 to 8 weeks and then again between 20 to
245 22 weeks, immediately after the second and third boosters (Figure 6B). The polyclonal immune
246 sera demonstrated sustained binding reactivity to the autologous Envelope trimer and with the
247 cross-clade Envelopes, though with a lower extent to heterologous Envs. The half-lives ($t1/2$) of

248 the immune sera titers against the autologous Env were significantly longer (p value: 0.007) as
249 compared to that of the heterologous Envs (SF162, 6240, 1086) tested. The overall immune sera
250 binding titers were comparable across the test groups; however, rabbits immunized with 330
251 SOSIP and ferritin NPs exhibited statistically significantly antibody titers (p value: 0.01)
252 compared to those immunized with NFL counterparts. Peak serum antibody binding to 330 Env
253 was observed at week 22, prompting further analysis of week 22 serum samples for their
254 neutralization activity.

255 Neutralization breadth was further evaluated against autologous (330.16.E6), closely
256 related (329.14.B1), and heterologous clade C (MW965.26 and 25925), Tier 1 clade B (SF162),
257 and Tier 2 clade A (BG505.T332N) pseudoviruses. No immune sera response was detected
258 against murine leukemia virus (MLV) used as a negative control and all animals exhibited
259 neutralizing antibody responses following immunization, except for one in the NFL group
260 (NZW5273) (Table S4). Multivalent 330 ferritin NPs and SOSIP elicited a strong neutralizing
261 response against autologous (330.16.E6) and closely related Envs (329.14.B1) as compared to
262 NFL counterpart. The Ferritin NP group elicited the most robust autologous neutralizing
263 antibody response, with a median $ID_{50}$ titer of 1160 compared to the soluble gp140 trimer
264 groups (SOSIP and NFL) exhibited median $ID_{50}$ titers of 830 and 375, respectively (Figure 6C).
265 The Ferritin NP group demonstrated a statistically significant increase in neutralizing antibody
266 titers compared to both the SOSIP ($p = 0.014691$) and NFL ($p = 0.010323$) groups, with fold
267 differences of 2.5-fold and 3.5-fold, respectively. These findings are consistent with the results
268 from the capture ELISA, where the NP and SOSIP groups exhibited sustained binding reactivity,
269 whereas the NFL group showed a decline in response after boosters. The NP and SOSIP groups
270 demonstrated moderate heterologous neutralizing responses against the clade C Tier 1 viruses
271 (MW965.26 and 25925) and the Tier 1 clade B virus (SF162), with responses comparable to each
272 other and higher than the NFL group although the differences were not statistically significant.
273 None of the 330 immunogens induced neutralizing responses against the Tier 2 BG505 virus,
274 which aligns with the low BG505 nAb activity observed in the plasma of the AIIMS_330 HIV-1-
275 infected elite neutralizer[35]. Overall, we observed that both 330 SOSIP Env trimer and ferritin NPs
276 elicited strong autologous NAb responses, as well as cross-clade neutralization, though with a
277 limited magnitude. Notably, the presentation of these antigens on ferritin NPs was associated
278 with a higher trend in NAb response induction.

279

280 **DISCUSSION**

281 HIV-1 clade-C accounts for more than half of global HIV-1 infections, with particularly
282 high prevalence in South Africa and India[19,20]. Comparative analyses of clade-C viruses from
283 these regions reveal the significant differences in their sequences, highlighting distinct
284 evolutionary trajectories[69]. These regional variations in intra-clade-C Env sequences likely
285 contribute to the differential sensitivity of circulating strains to HIV-1 nAbs. HIV-1 Clade-C
286 characterized by unique features such as enhanced transmission efficiency, extensive genetic
287 diversity within the V1-V3 region of the Env gene, and a distinct profile of drug resistance
288 mutations compared to other clades[69–72]. Understanding these differences is crucial for tailoring
289 the prevention and treatment strategies in clade C prevalent regions[19,20]. Structural information
290 on the HIV-1 Env trimer from clade-C is crucial for structure-guided immunogen design.
291 However, only a limited number of high-resolution structures are available for native-like clade-
292 C Env trimers, such as 16055[50,73], DU172.17[74], 426c[75], and CZA97.12[76]. Although many HIV-1 Env
293 immunogens have been stabilized, most studies have extensively characterized BG505, a Clade-A
294 transmitted founder Env derived from a 6-week-old infant with elite neutralizing activity[11]. Such
295 elite individuals from the pediatric group could provide valuable Env immunogen templates, as
296 HIV-1 infection and disease progression in children differs from that in adults[31,34,35]. Notably,
297 neutralizing antibodies tend to arise early in the course of infection in pediatric individuals, with
298 the ability to neutralize contemporaneous viral Envelopes[33,37]. We previously reported a pair of
299 monozygotic twins (AIIMS_329 and AIIMS_330) with elite neutralizing activity, whose plasma
300 demonstrated exceptionally potent bNAb responses with multi-epitope specificities against a
301 diverse panel of multi-clade heterologous Env pseudoviruses[33,35]. These Envs hold significant
302 potential as templates for vaccine design and as antigenic baits to isolate HIV-1 bNAbs for
303 immunotherapeutic applications[49]. Recent studies demonstrated that, multimeric presentation
304 of viral class I fusion viral glycoproteins, such as , Ebola virus Glycoprotein (GP)[77,78], influenza
305 hemagglutinin (HA)[79,80], Respiratory Syncytial Virus (RSV) F protein[81,82], SARS-CoV-2 S
306 protein[83–86] and HIV-1 Env[29, 30] on ferritin NPs has enabled the efficient production of well-
307 ordered NP-based vaccine candidates with a capacity to induce robust immune response.

308 Herein, we designed and characterized a soluble HIV-1 clade-C 330 Env trimer on SOSIP
309 and NFL platform, derived from a circulating virus in an Indian pediatric EN AIIMS_330[35], by
310 stabilizing the Env using version 7 mutations and displaying the SOSIP Env on self-assembling
311 ferritin NPs[29,30]. The purification yield of Env trimers post SEC was around ~1 mg/L for SOSIP

312 and ~1.45 mg/L for NFL, which was higher or comparable to the Indian and South African Clade-
313 C strains (CZA97: ~0.4-0.6 mg/mL, 329 SOSIP: ~0.6 mg/mL, 16055 NFL: ~2 mg/mL, 1PGE-
314 THIVC SOSIP)[23,48–50]. Using Negative stain Electron Microscopy, we demonstrated that SOSIP and
315 NFL Envs displaying key features of native-like trimeric conformation and Env trimers were
316 presented efficiently on ferritin NPs as observed in stabilized BG505 Env-particles[29]. The
317 structure of the 330 SOSIP, resolved by single-particle cryo-EM, revealed trilobular Env
318 structures in their prefusion, closed conformation. The generated Env trimer and particles
319 displays a desirable antigenic profile, with nanomolar affinity to conformation specific bNAbs
320 (PGT145 & PGT151), with negligible reactivity to non-nAbs (F105 & 17b+sCD4), shielding the
321 Env immunodominant regions. Biophysical characterization showed that the 330 Env exhibits a
322 balanced thermodynamic profile and high degree of thermal stability with a Tm of ~74°C which
323 is notably higher as compared to other reported clade C Envs ZM197 (69°C)[12] , IPGE-THIVC
324 (62°C)[23] and 16055 (68°C)[87]. We observed greater structural similarity of 330 Env to clade-A
325 BG505 Env (RMSD gp120-0.685 Å & gp41-0.478 Å) compared to clade-B AMC009 Env reported
326 (RMSD gp120-2.623 Å & gp41-1.624 Å), suggesting well-ordered structures[14]. Cryo-EM
327 structure of 330 Env in complex with autologous bNAb 44m revealed the well-exposed epitopes;
328 the three trilobular structures occupied by the three Fab arms as observed with BG505-44m
329 structure. We identified herein, additional key antigenic determinants T144 and T413 in the
330 autologous 330 Env, that interacted with 44m; , in addition to D325 and N322 dependency, as
331 observed with heterologous BG505 Env[36]. Our findings offer crucial insights into the antigenic
332 determinants in the clade C virus Env, that interact with the autologous antibody 44m, that can
333 inform a clade-based vaccine design. Furthermore, using a reverse vaccinology approach, these
334 insights can guide the structure-based engineering of neutralizing antibodies[88].
335
336 Rabbit immunizations demonstrated that the 330 Env immunogens elicited robust
337 immune responses against autologous and other tier-1 viruses, with limited cross-clade
338 neutralization. This may be attributed to distinct antigenic determinants on heterologous Envs,
339 adjuvant used or by varied glycan compositions[89,90]. Further insight can be achieved by
340 investigating the specific epitopes targeted by NAbs in the immune sera, however it has not been
341 addressed herein and is a limitation of this study. The multivalent presentation of HIV-1 antigens
342 on ferritin NPs correlated with enhanced neutralization potency, likely attributed to augmented
343 B-cell activation signals[91]. This observation aligns with findings from germline-targeting eOD-
344 GT8 NPs, suggesting a potential mechanism for eliciting more robust and coordinated immune

345 responses[91]. These findings emphasize the need for further exploration of the role of glycans and
346 structure guided mutations in shaping immunogenicity.

347 In summary, we designed and characterized soluble HIV-1 Env trimers derived from a
348 clade-C-infected pediatric elite-neutralizer from India. Structural analysis of the 330 Env trimer
349 in complex with autologous the bNAb 44m-a heavy chain matured version of the first bNAb
350 identified from AIIMS_330 donor, revealed molecular features of 330 Env-44m bNAb interaction
351 which could inform structure-based vaccine design. Our findings indicate that the 330 SOSIP Env
352 trimer can serve as a valuable antigenic probe for bNAb discovery and that both the SOSIP and
353 ferritin nanoparticle versions represent promising candidates for multivalent HIV-1 vaccine
354 design and development.

355 **MATERIALS AND METHODS**

356 **Institutional Review Board & Ethics approval**

357 This study was conducted after obtaining approval from the institutional ethics committee, All
358 India Institute of Medical Sciences (AIIMS), New Delhi, India (250/IAEC-1/2020). Rabbit
359 immunization was outsourced to a contract research organization (CRO) Liveon Biolabs Private
360 Limited, Bengaluru, Karnataka, India with IAEC (IAEC-approved protocol No.: LBPL-IAEC-008-
361 01/2021; study number: LBPL/NG-1736 (EF)). The immunization studies described here were
362 carried out on female naive New Zealand White rabbits of 2.0–2.5 kg and aged 4 months. All
363 animal experiments adhered to the guidelines for the care and use of laboratory animals as
364 outlined by the Committee for Control and Supervision of Experiments on Animals (CCSEA),
365 Government of India[92].

366 **Construct design**

367 The 330 Env gene was derived from a previously identified Indian clade C HIV-1 Env (330.16.E6,
368 GenBank: MK076720) obtained from a pediatric elite-neutralizer AIIMS_330, as previously
369 described[35]. The 330 Env construct were design in soluble forms as SOSIP.664[11] gp120-gp41
370 cleaved Env trimers and NFL.664[38] gp140 single-chain Env trimers along with tailoring of SOSIP
371 Env trimers on self-assembling ferritin nanoparticles[29] to achieve multivalency. SOSIP & NFL
372 constructs were stabilize by incorporating I559P & ΔMPER (Env prefusion stabilizing
373 mutation)[42,43], R315Q (reduced V3 non-nAb immunodominant exposure)[44], I201C-A433C
374 (intraprotomer locking disulfide bond, reduced V3 exposure)[12], and clade C stabilizing B505-

375 Trimer Derived (TD8) mutations (E47D, T49E, V65K, I165L, K429R, K432Q, K500R)[39]. The SOSIP
376 construct was designed by introducing an SOS disulfide bond (A501C-T605C)[46], an I559P
377 mutation[42], and an optimized furin cleavage site (RRRRRR)[47]. In contrast, the NFL (Native
378 Flexible Linker) construct retained the I559P mutation and linked gp120 and gp41 using a
379 flexible glycine-serine linker (GGGGSGGGGS)[38]. Native signal sequence is replaced by the CD5
380 signal peptide (MGSLQPLATLYLLGMLVASVLA) for enhanced secretion of Envelope proteins,
381 constructs were codon optimized for mammalian expression and synthesized commercially by
382 GeneArt (Thermo Fischer Scientific). For binding assays, 330 Env constructs were tagged with
383 either a His-tag (GSGSGGSGHHHHHHHH) or a twin strep tag (tst)
384 (WSHPQFEKGGGSGGGSWSHPQFEK) at the C-terminus of gp41ECTO, preceding the stop codon.
385 These constructs were subsequently cloned into pPI4 expression vector using Pst1 and Not1
386 restriction sites. The 330 ferritin NP's construct was generated by fusing the N-terminus from
387 *Helicobacter pylori* ferritin (GenBank: WP_000949190.1), starting from Asp5 to Ser167, to the
388 SOSIP.664 C-terminus (truncated at position 664), separated by a Gly-Ser (GSG) linker, as
389 described previously[29].

390 **Envelope Protein Expression**

391 The 330 Env encoding plasmids were transiently expressed in 293F suspension cells (Gibco,
392 R790-07). 293F cells were thawed and maintained in Freestyle Expression Medium (Gibco,
393 K9000-01) in a Shaker incubator at 37°C, with 120 r.p.m. and 8% CO2. For transfection, HIV-1
394 Env and furin protease encoding plasmids mixed in a 3:1 ratio (w/w) with NFL (500 μg), SOSIP
395 Env (333.3 μg), to furin (166.6 μg) incubated with transfection reagent PEImax (Polysciences,
396 24765) in a 3:1 ratio (w/ w) PEI max to DNA for 20 min at room temperature (RT) and then
397 added to 1L culture at density of 1 million cells/mL. Seven days post-transfection, the
398 supernatants were harvested, centrifuged, and filtered using 0.45-mm filters (Nalgene,
399 2954545).

400 **Envelope Protein Purification**

401 330 SOSIP Env and SOSIP Env-NP fusion proteins were purified by PGT145 bNAb
402 immunoaffinity chromatography, as described previously[48]. Briefly, HIV-1 pre-fusion closed
403 trimer-specific bNAb PGT145[93] was covalently coupled to the CNBr-activated Sepharose 4B
404 beads (GE Healthcare, 17043001) according to the manufacturer's protocol for antibody
405 coupling. The PGT145-coupled CNBr Sepharose 4B bead column was used to purify HIV-1 Env

406 trimers or Env trimer NPs. Env proteins contained in Expi293F filtered supernatants were
407 captured on PGT145-coupled CNBr-activated sepharose beads by overnight rolling incubation at
408 4 °C. Subsequently, the mixture of supernatants and beads was passed over Econo-columns
409 (Biorad, 7371512). The columns were then washed with three column volumes of 0.5 M NaCl
410 and 20 mM Tris HCl pH 8.0 solution. After elution with 3 M $MgCl_2$ pH 7.5, the proteins were
411 buffer-exchanged into TN75 (75 mM NaCl, 20 mM Tris HCl pH 8.0) or PBS buffer by
412 ultrafiltration with Vivaspin concentrators MWCO 100 kDa (Cytivia, 28932363). Protein
413 concentrations were determined from the A280 values measured using a NanoDrop One
414 (Thermo Fisher Scientific, 29018226) and the molecular weight and extinction coefficient values
415 were calculated by the ProtParam Expasy webtool. Env proteins used for immunization were
416 first purified using PGT145 affinity chromatography, followed by size-exclusion chromatography
417 (SEC) on a Superdex 200 Increase 10/300 GL column (28990944, GE Healthcare Life Sciences)
418 using an Äkta Pure 25M system (Cytiva, 29018226). Envs containing fractions were pooled,
419 concentrated, filter-sterilized, snap-frozen in liquid nitrogen, and stored at -80°C until further
420 use.

421 **SDS-PAGE and BN-PAGE Analyses**

422 For SDS-PAGE and blue native polyacrylamide gel electrophoresis (BN-PAGE) analyses, 2 µg of
423 330 gp140 Env trimers, or equimolar amounts of ferritin NP's (2.5 µg) was ran over precast
424 native gel 4–20 % Bis-Tris gradient gel (Biorad, 4561094). The degree gp120-gp41 cleavage was
425 examined by incubating the SOSIP & NFL protein with 0.1M dithiothreitol (DTT) and analysed by
426 SDS-PAGE under reducing conditions. Subsequently, gels were stained with the Colloidal Blue
427 Staining Kit (Invitrogen, LC6025), respectively.

428 **Enzyme linked Immunosorbent assay (ELISA)**

429 ELISAs were performed as previously described[94] using tst-tagged Env constructs on
430 StrepTactinXT-coated microplates (IBA Lifesciences, 2-4101-001). Purified proteins (1 µg/mL)
431 were diluted in NaHCO3 buffer and immobilized on 96-well Streptactin plates by O/N incubation
432 at 4°C. Following a three wash step with PBST (0.05% Tween20) to remove unbound trimers,
433 plates were blocked by 1% BSA in PBST for 2 hours at RT. Further the serial dilutions of test
434 antibodies ranging from 10ug – 0.004 ug/ml in PBST/1% BSA solution were added and
435 incubated for 2 h. After 3 washes with PBST, HRP-labelled goat anti-human IgG (Jackson
436 ImmunoResearch, AB_2337578) diluted 1:3000 in PBST/1% BSA was added and incubated for

437 30 mins, followed by 3 washes with PBST and 3 washes of PBS. A developing solution (1% TMB
438 (Mabtech, 3652-F10), allowed the colorimetric reaction, which was stopped by the addition of 2
439 N H2SO4. Finally, colour development (absorption at 450 nm, OD450) was measured at
440 NanoDrop One (Thermo Fisher Scientific, 29018226) to obtain the different binding curves.

441 **Biolayer Interferometry (BLI)**

442 Binding kinetics were measured using an Octet K2 (ForteBio, RED96e) device at RT with 1000
443 rpm agitation. Anti-human Fc sensors (Sartorius AHC, 18-5060) were used to capture mAbs on
444 the Octet K2, were equilibrated in kinetics buffer for 60 s to obtain a baseline prior to protein
445 association. 330 Envelope protein was used as analyte in concentrations ranging from 210 to 2.6
446 nM in the HEPES buffer (pH 7.2) background supplemented with 0.02% Tween 20 and 0.1%
447 BSA. Binding was assessed by incubating mAb-captured sensors in wells containing 10 µg/ml
448 Env for 120 seconds with 1000 rpm agitation. Association was recorded for 150 s followed by
449 dissociation for 450 s. Data were analysed using the ForteBio Data analysis software (Forte- Bio
450 Inc, Version 9.0) and a global fit was performed using a 1:1 binding model to fit the association
451 and dissociation curves.

452 **Sypro orange differential scanning fluorimetry (DSF)**

453 330 SOSIP protein were prepared at a concentration of 0.2 mg/mL in 1XPBS and transferred into
454 0.1 mL polypropylene PCR tube strips (Tarsons, 611020) with a final volume of 25 µL. Sypro
455 Orange protein stain (Invitrogen, 4461146) was added at a 1:200 dilution. The samples were
456 analyzed using a Rotor-Gene Q system (Qiagen, 9001862) with a high-resolution melt (HRM)
457 protocol, starting at 25°C and increasing to 90°C in 1°C increments, with each step lasting 4
458 seconds. Melt curve data were processed using Rotor-Gene Q Series Software.

459 **Circular dichroism (CD) spectroscopy**

460 The Far-UV spectrum was recorded in the wavelength range of 200–250 nm using a CD
461 Spectrophotometer (JASCO, J-1500) with a 0.1 cm path length Quartz cuvette (Sigma Aldrich,
462 I0285). Measurements were conducted for the 330 protein in a 20 mM phosphate buffer (pH 7.5)
463 with100 mM NaCl concentration at 4˚C for 30 minutes. Each spectral scan was averaged over 2–3
464 measurements. The CD spectra were visualized using SigmaPlot 10.0, and the secondary
465 structure was analyzed through the BESTSEL online server. For thermal studies, measurements

466 were performed between 20˚C and 80˚C using the same Quartz cuvette, and the melting curve
467 was generated using SigmaPlot 10.0.

468 **Negative Stain Microscopy (NS-EM)**

469 Negative-stain electron microscopy (NS-EM) was performed essentially as described
470 elsewhere[95]. Briefly, 3 µl of purified 330 gp140 Env trimers or ferritin NPs (~0.03 mg/mL) were
471 applied to glow discharged (20 mA for 30 s) carbon-coated 400 Cu mesh grid. After 5 s, grids
472 were negatively stained with 2% (w/v) uranyl formate for 60 s. Imaging was performed using a
473 120 kV Talos L120C electron microscope (TALOSL120CMS) equipped with a 4k x 4k Ceta camera
474 at a magnification of 73kx (3.84 Å/pixel). The collected images were processed in EMAN 2.1[96].
475 Particle extraction and reference-free 2D class averages were generated using simple_prime2D
476 in SIMPLE 2.1 software[97] with a mask diameter of 30 pixels at 3.84 Å/pix.

477 **Preparation of 44m Fab fragment**

478 Fab fragments were generated from 4 mg of AIIMS-44m IgG using a Fab fragmentation kit (G
479 Biosciences, 786-273) following the manufacturer's protocol. Briefly, 0.5 ml of 44m IgG was
480 desalted using a SpinOUT™ GT-600 column. Cysteine.HCl was added to the Fab Digestion Buffer
481 (pH) to a final concentration of 20 mM before papain digestion. The 0.5 ml IgG sample was then
482 incubated with Immobilized Papain in the spin column at 37°C for 6 hours with end-over-end
483 mixing. After incubation, the digested antibody solution was collected by centrifugation at 5,000
484 x g for 1 minute. The flow-through was further incubated with Protein A resin for 10-15 minutes
485 at room temperature (RT) with end-over-end mixing. Subsequently, the Fab fragments were
486 collected in the flow-through while Fc fragments and undigested IgG remained bound to the
487 resin. The purity and size of the Fab fragments were assessed by SDS-PAGE and the purified Fab
488 fragments were stored at -80°C.

489 **Cryo-EM sample preparation, data acquisition, data analysis and model fitting**

490 330 Env trimer (1.5 mg/ml) incubated with 44m Fab at 1:3 molar ratio. 3 µl of sample were
491 applied to glow discharged R1.2/R1.3 300 mesh copper grids and immediately blotted for 8 secs
492 without any blotting force using FEI Vitrobot Mark IV plunger at 22°C. The grid was immediately
493 plunge-frozen into liquid ethane at liquid nitrogen temperature. Cryo-EM data were collected
494 using 200 kV Talos Arctica transmission electron microscope (Thermo Scientific,
495 TALOSARCTICA) equipped with Gatan K2 Summit Direct Electron Detector. Movies were

496 recorded automatically using Latitude-S (DigitalMicrograph - GMS 3.5) at a nominal
497 magnification of 45,000x at the effective pixel size of 1.17 Å[97]. Micrographs were acquired in
498 counting mode with a total dose of 60 $e^-/Å^2$, with an exposure time of 8 sec distributed for 20
499 frames. A total of 5215 movies were acquired for the 330 SOSIP Env trimer and 44m Fab
500 complexes, respectively. Single-Particle Analysis (SPA) was performed for the acquired Cryo-EM
501 movies using the Relion version 3.1[98] and CryoSPARC v4.2.1[99]. At first, drift and gain corrections
502 of the individual movies were performed with MotionCorr2[100] and estimated Contrast transfer
503 function (CTF) parameters using CTFFIND 4.1.13 in Relion[101]. Subsequently, CTF-estimated
504 micrographs were subjected to analysis to eliminate bad micrographs using cisTEM[102], and also
505 to remove poor resolution micrographs with a fit resolution threshold of 7 Å. The particles from
506 the best micrographs were chosen for automated picking using 2D reference in Relion and
507 extracted with the box sizes of 320 pixels for the 44m Fab bound 330 SOSIP Env trimer
508 complexes. The extracted particles were imported to CryoSPARC v4.2.1, and the rest of the
509 processing was performed there. After four rounds of rigorous 2D classification, 879,956
510 particles were selected from the best 2D classes with high-resolution features of the Ab-bound
511 complex. This dataset was divided into 6 classes for Ab initio reconstruction with C3 symmetry.
512 The class04, with 109004 particles, had the best Ab bound features among all the classes (Figure
513 S6). Therefore, we considered the class04 for non-uniform refinement by imposing C3 symmetry.
514 The class04 was further refined by local refinement, and the resolution of the 3D map was
515 estimated at FSC 0.143. For model fitting, the Cryo-EM maps of 330 Env trimers were docked on
516 ferritin structure (PDB: 3BVE) symmetrically on four sites. Overviews of Cryo-EM data
517 processing are shown in S. Table S3.

518 **Immunizations**

519 The rabbit immunization studies were conducted at a contract research organization (CRO),
520 Liveon Biolabs Private Limited, Karnataka, India, under GLP-compliant conditions. Liveon
521 Biolabs is an AAALAC International-accredited facility and is registered with the CCSEA,
522 Government of India. Female, naive New Zealand White rabbits, aged 4 months and weighing
523 between 2.0–2.5 kg, were used for the study. The protocol for animal use was approved by the
524 Institutional Animal Ethics Committee (IAEC) of Liveon Biolabs (Approval No.: LBPL-IAEC-008-
525 01/2021; Study No.: LBPL/NG-1736 (EF)). Prior to housing, the experimental room underwent
526 fumigation for decontamination, and microbial load was assessed using the settle plate method.
527 The rabbits were kept in a temperature-controlled Environment (20 ± 3 °C) with relative

528 humidity ranging from 30–70%, a 12-hour light/dark cycle, 12–15 air changes per hour, and a
529 noise level below 80 dBs. Mortality and morbidity were monitored twice daily, while clinical
530 observations were conducted at least once per day throughout the study. Body weight
531 measurements were recorded for all animals prior to the administration of the test item on Day
532 1 and subsequently on a weekly basis (±1 day) during the treatment period. The gp140 SOSIP
533 and NFL Env immunogens (G1 and G2) were administered at a dose of 20 µg of trimers, or an
534 equivalent molar amount SOSIP-ferritin nanoparticles (25 µg) (G3) formulated with the AddaVax
535 adjuvant (1:1 v/v) (vac-adx-10, Invivogen). The placebo group (G4) received only adjuvant with
536 sterile 1XPBS. Doses were calculated based on the molecular weight of the protein peptides,
537 excluding glycans, as described elsewhere[66,66]. Blood samples were collected from rabbits at
538 weeks 0, 4, 6, 16, 20, and 22. Before blood collection from the marginal ear vein, a local
539 anaesthetic cream containing 4% lidocaine was applied for 5 minutes. The immunization
540 process, including bleeding protocols, caused minimal and brief pain or distress, with no
541 significant impact on animal health. At the end of the experimental period, the rabbits were
542 euthanized using a lethal dose of sodium thiopental. Complement-deactivated serum samples
543 were subsequently analysed for their binding reactivity and neutralization potential.

544 **HIV-1 pseudovirus generation**

545 The HIV-1 pseudoviruses were produced in HEK293T cells as described previously[103] by co-
546 transfecting the corresponding full HIV-1 gp160 Envelope plasmid and a pSG3ΔEnv backbone
547 plasmid. Briefly, $1 \times 10^5$ cells in 2 mL complete DMEM (10% fetal bovine serum (FBS) (Gibco,
548 26140079 and 1% penicillin and streptomycin (Gibco, 15140-122) were seeded per well of a 6-
549 well cell culture plate (Costar, 3506) the day before transfection. For transfection, Envelope
550 (1.25 µg) and delta Envelope (pSG3ΔEnv backbone) plasmids (2.50 µg) were mixed in a 1:2 ratio
551 in Opti-MEM (Gibco, 31985062), with a final volume of 200 µL per well, and incubated for 5 min
552 at room temperature. Next, 3 µL of PEI-Max transfection reagent (Polysciences, 24765) (1
553 mg/mL) was added to this mixture before further incubation for 15 min at room temperature.
554 This mixture was then added dropwise to the HEK 293T cells supplemented with fresh complete
555 DMEM growth media and incubated at 37 °C for 48 h. Pseudoviruses were then harvested by
556 filtering cell supernatants with 0.45 µm sterile filters (mdi), aliquoted, and stored at −80 °C until
557 usage.

558

559 **HIV-1 Neutralization assay**

560 Neutralization assays were carried out using TZM-bl reporter cells which is described
561 elsewhere[104]. The autologous and heterologous NAb response of end point sera was measured in
562 TZM-bl cell neutralization assays. Neutralization was measured as a reduction in luciferase gene
563 expression after a single round of infection of TZM-bl cells (NIH AIDS Reagent Program) with
564 HIV-1 Env pseudoviruses. The $TCID_{50}$ of the HIV-1 pseudoviruses was calculated and 200 $TCID_{50}$
565 of the virus was used in the neutralization assays through incubation with three-fold serially
566 diluted rabbit sera starting at a 1:20 dilution. Next, freshly trypsinized TZM-bl cells in a complete
567 DMEM (10% fetal bovine serum (FBS) (Gibco, 26140079 and 1% penicillin and streptomycin
568 (Gibco, 15140-122) containing 50 µg/mL DEAE-dextran (Sigma, D9885) at $10^5$ cells/well were
569 added and the plates were incubated at 37 °C for 48 h. Virus controls (cells with HIV-1 virus
570 only) and cell controls (cells without virus and antibody) were included. MuLV was used as a
571 negative control. After the incubation of the plates for 48 h, luciferase activity was measured
572 using the Bright-Glow Luciferase Assay System (Promega, E2610). $ID_{50}$ for antibodies were
573 calculated from a dose–response curve fit with a non-linear function using GraphPad Prism 8
574 software (San Diego, CA, USA). All neutralization assays were repeated at least 2 times, and the
575 data shown are from representative experiments.

576 **Statistical analysis**

577 Statistical significance between groups and subgroups was assessed using the Mann–Whitney U
578 test, Student's t-test, and one-way analysis of variance for continuous variables. For
579 representative results, experiments was done in replicates or repeated twice. All statistical
580 analyses and plotting were performed using GraphPad Prism (version 8.0; La Jolla, CA, USA)

581 **FUNDING**

582 This study was funded by the Department of Biotechnology (DBT), India
583 (BT/PR39156/DRUG/134/91/2021, BT/PR30120/MED/29/1339/2018) grants awarded to K.L.
584 This work was also supported by Department of Science & Technology-FIST (SR/FST/LSII-
585 039/2015) and DBT-BUILDER Program (BT/INF/22/SP22844/2017) grants awarded to S.D. S.K.
586 is supported by the DBT-Wellcome Trust India Alliance Early Career Fellowship Grant
587 IA/E/18/1/504307. The funders played no role in the study design, data collection, analysis, or
588 interpretation, nor in the writing of the manuscript or the decision to publish the results.

589 **ACKNOWLEDGMENTS**

590 The authors are grateful to the NIH AIDS reagent program for providing the HIV-1 research
591 reagents and the Neutralizing Antibody Consortium (NAC), IAVI, USA for providing the HIV-1
592 neutralizing antibodies donated by Michel Nussenzweig, Hermann Katinger, Mark Connors,
593 James Robinson, Dennis Burton, John Mascola, Peter Kwong, and William Olson. We express
594 gratitude to Prof. R.W. Sanders for generously providing the PPI4 expression vector and the
595 training provided to S.D.S as a part of his HIV-1 Trust Fellowship. We appreciate the support of
596 Liveon Biolabs for conducting the immunization studies. We also extend our appreciation for the
597 IAVI-Leader Development Program awarded to S.D.S.

598 **AUTHOR CONTRIBUTIONS**

599 Conceptualization and implementation; S.D.S., S.Ku, and K.L., EM work & data acquisition; S.D.S.,
600 A.C., Formal analysis; S.D.S., S.Ku, K.L., S.D., Biophysical analysis; A.C., S.D.S., L.M., B.M., E.A.S.,
601 Expression and purifications: S.D.S., A.R., I.A., S.S., V.I., A.G., T.B., & R.Ku., ELISA & neutralization
602 assays; S.D.S., S.S, A.R., S.Ka, A.W.H., Animal studies; S.D.S., S.Ka, H.B., A.G., & A.W.H. Octet
603 experimentation; S.D.S., R.Ku., S.A., and M.P., Original manuscript writing; S.D.S., S.Ku, A.C., & K.L.,
604 Supervision; S.D., & K.L., Project administration; S.D.S. & S.Ku, funding acquisition; S.D., & K.L. All
605 authors have read and agreed to the published version of the manuscript.

606 **CONFLICT OF INTERESTS**

607 An Indian patent application (202211004612) has been filed on the 330 SOSIP Env trimer
608 described in this study. The following authors: K.L., S.D.S., S.Ku. and S.S. are listed as inventors on
609 the patent. The other authors declare no conflicts of interest.

610 **DATA AVAILABILITY**

611 The modified 330 Envelope protomer sequence been deposited in GenBank with accession
612 number XXXX. Cryo-EM maps & atomic coordinates of reported structures are deposited into the
613 Electron Microscopy Data Bank (EMDB) with accession code EMD: XXXX for 330 SOSIP Env
614 trimer in complex with bNAb 44m. Any additional data are available upon reasonable request
615 from the corresponding authors.

616

617 **REFERENCES**


618 1. Burton, D. R. *et al.* A Blueprint for HIV Vaccine Discovery. *Cell Host Microbe* **12**, 396–407
619 (2012).
620 2. Simek, M. D. *et al.* Human Immunodeficiency Virus Type 1 Elite Neutralizers: Individuals with
621 Broad and Potent Neutralizing Activity Identified by Using a High-Throughput Neutralization
622 Assay together with an Analytical Selection Algorithm. *J. Virol.* **83**, 7337–7348 (2009).
623 3. van den Kerkhof, T. L. G. M. *et al.* Early development of broadly reactive HIV-1 neutralizing
624 activity in elite neutralizers. *AIDS* **28**, 1237 (2014).
625 4. Mascola, J. R. *et al.* Protection of macaques against vaginal transmission of a pathogenic HIV-
626 1/SIV chimeric virus by passive infusion of neutralizing antibodies. *Nat. Med.* **6**, 207–210
627 (2000).
628 5. Mascola, J. R. *et al.* Protection of Macaques against pathogenic simian/human
629 immunodeficiency virus 89.6PD by passive transfer of neutralizing antibodies. *J. Virol.* **73**,
630 4009–4018 (1999).
631 6. Parren, P. W. *et al.* Antibody protects macaques against vaginal challenge with a pathogenic
632 R5 simian/human immunodeficiency virus at serum levels giving complete neutralization in
633 vitro. *J. Virol.* **75**, 8340–8347 (2001).
634 7. Moldt, B. *et al.* Highly potent HIV-specific antibody neutralization in vitro translates into
635 effective protection against mucosal SHIV challenge in vivo. *Proc. Natl. Acad. Sci. U. S. A.* **109**,
636 18921–18925 (2012).
637 8. Hessell, A. J. *et al.* Broadly neutralizing human anti-HIV antibody 2G12 is effective in
638 protection against mucosal SHIV challenge even at low serum neutralizing titers. *PLoS*
639 *Pathog.* **5**, e1000433 (2009).
640 9. Karasavvas, N. *et al.* The Thai Phase III HIV Type 1 Vaccine Trial (RV144) Regimen Induces
641 Antibodies That Target Conserved Regions Within the V2 Loop of gp120. *AIDS Res. Hum.*
642 *Retroviruses* **28**, 1444–1457 (2012).
643 10. Kim, J., Excler, J.-L. & Michael, N. Lessons from the RV144 Thai Phase III HIV-1 Vaccine Trial
644 and the search for correlates of protection. *Annu. Rev. Med.* **66**, (2014).
645 11. Sanders, R. W. *et al.* A Next-Generation Cleaved, Soluble HIV-1 Env Trimer, BG505 SOSIP.664
646 gp140, Expresses Multiple Epitopes for Broadly Neutralizing but Not Non-Neutralizing
647 Antibodies. *PLOS Pathog.* **9**, e1003618 (2013).

648 12. Torrents de la Peña, A. *et al.* Improving the Immunogenicity of Native-like HIV-1 Envelope
649 Trimers by Hyperstabilization. *Cell Rep.* **20**, 1805–1817 (2017).
650 13. Torrents de la Peña, A. *et al.* Immunogenicity in Rabbits of HIV-1 SOSIP Trimers from Clades
651 A, B, and C, Given Individually, Sequentially, or in Combination. *J. Virol.* **92**, (2018).
652 14. Schorcht, A. *et al.* Neutralizing Antibody Responses Induced by HIV-1 Envelope Glycoprotein
653 SOSIP Trimers Derived from Elite Neutralizers. *J. Virol.* **94**, 10.1128/jvi.01214-20 (2020).
654 15. de Taeye, S. W. *et al.* Immunogenicity of Stabilized HIV-1 Envelope Trimers with Reduced
655 Exposure of Non-neutralizing Epitopes. *Cell* **163**, 1702–1715 (2015).
656 16. Sok, D. *et al.* Rapid elicitation of broadly neutralizing antibodies to HIV by immunization in
657 cows. *Nature* **548**, 108–111 (2017).
658 17. Sanders, R. W. *et al.* HIV-1 VACCINES. HIV-1 neutralizing antibodies induced by native-like
659 Envelope trimers. *Science* **349**, aac4223 (2015).
660 18. Houser, K. V. *et al.* Safety and immunogenicity of an HIV-1 prefusion-stabilized Envelope
661 trimer (Trimer 4571) vaccine in healthy adults: A first-in-human open-label, randomized,
662 dose-escalation, phase 1 clinical trial. *eClinicalMedicine* **48**, (2022).
663 19. Gartner, M. J., Roche, M., Churchill, M. J., Gorry, P. R. & Flynn, J. K. Understanding the
664 mechanisms driving the spread of subtype C HIV-1. *EBioMedicine* **53**, 102682 (2020).
665 20. Hemelaar, J., Gouws, E., Ghys, P. D. & Osmanov, S. Global and regional distribution of HIV-1
666 genetic subtypes and recombinants in 2004. *AIDS Lond. Engl.* **20**, W13-23 (2006).
667 21. Ahmed, S. *et al.* Stabilization of a soluble, native-like trimeric form of an efficiently cleaved
668 Indian HIV-1 clade C Envelope glycoprotein. *J. Biol. Chem.* **292**, 8236–8243 (2017).
669 22. Rutten, L. *et al.* A Universal Approach to Optimize the Folding and Stability of Prefusion-
670 Closed HIV-1 Envelope Trimers. *Cell Rep.* **23**, 584–595 (2018).
671 23. Kumar, R. *et al.* Elicitation of potent serum neutralizing antibody responses in rabbits by
672 immunization with an HIV-1 clade C trimeric Env derived from an Indian elite neutralizer.
673 *PLOS Pathog.* **17**, e1008977 (2021).
674 24. Kumar, S. *et al.* Design and immunogenicity of an HIV-1 clade C pediatric Envelope
675 glycoprotein stabilized by multiple platforms. *BioRxiv Prepr. Serv. Biol.* 2024.09.14.613016
676 (2024) doi:10.1101/2024.09.14.613016.
677 25. Schiller, J. & Chackerian, B. Why HIV Virions Have Low Numbers of Envelope Spikes:
678 Implications for Vaccine Development. *PLOS Pathog.* **10**, e1004254 (2014).

679 26. Zhao, Q., Li, S., Yu, H., Xia, N. & Modis, Y. Virus-like particle-based human vaccines: quality
680 assessment based on structural and functional properties. *Trends Biotechnol.* **31**, 654–663
681 (2013).
682 27. Ludwig, C. & Wagner, R. Virus-like particles-universal molecular toolboxes. *Curr. Opin.*
683 *Biotechnol.* **18**, 537–545 (2007).
684 28. Jennings, G. T. & Bachmann, M. F. The coming of age of virus-like particle vaccines. *Biol. Chem.*
685 **389**, 521–536 (2008).
686 29. Sliepen, K. *et al.* Presenting native-like HIV-1 Envelope trimers on ferritin nanoparticles
687 improves their immunogenicity. *Retrovirology* **12**, 82 (2015).
688 30. He, L. *et al.* Presenting native-like trimeric HIV-1 antigens with self-assembling nanoparticles.
689 *Nat. Commun.* **7**, 12041 (2016).
690 31. Goo, L., Chohan, V., Nduati, R. & Overbaugh, J. Early development of broadly neutralizing
691 antibodies in HIV-1–infected infants. *Nat. Med.* **20**, 655–658 (2014).
692 32. Ditse, Z. *et al.* HIV-1 Subtype C-Infected Children with Exceptional Neutralization Breadth
693 Exhibit Polyclonal Responses Targeting Known Epitopes. *J. Virol.* **92**, (2018).
694 33. Kumar, S. *et al.* An HIV-1 Broadly Neutralizing Antibody from a Clade C-Infected Pediatric
695 Elite Neutralizer Potently Neutralizes the Contemporaneous and Autologous Evolving
696 Viruses. *J. Virol.* **93**, e01495-18 (2019).
697 34. Makhdoomi, M. A. *et al.* Neutralization resistant HIV-1 primary isolates from antiretroviral
698 naïve chronically infected children in India. *Virology* **499**, 105–113 (2016).
699 35. Mishra, N. *et al.* Viral Characteristics Associated with Maintenance of Elite Neutralizing
700 Activity in Chronically HIV-1 Clade C-Infected Monozygotic Pediatric Twins. *J. Virol.* **93**,
701 e00654-19, /jvi/93/17/JVI.00654-19.atom (2019).
702 36. Kumar, S. *et al.* Recognition determinants of improved HIV-1 neutralization by a heavy chain
703 matured pediatric antibody. *iScience* **26**, 107579 (2023).
704 37. Simonich, C. A. *et al.* HIV-1 Neutralizing Antibodies with Limited Hypermutation from an
705 Infant. *Cell* **166**, 77–87 (2016).
706 38. Sharma, S. K. *et al.* Cleavage-Independent HIV-1 Env Trimers Engineered as Soluble Native
707 Spike Mimetics for Vaccine Design. *Cell Rep.* **11**, 539–550 (2015).
708 39. Guenaga, J. *et al.* Structure-Guided Redesign Increases the Propensity of HIV Env To Generate
709 Highly Stable Soluble Trimers. *J. Virol.* **90**, 2806–2817 (2015).
710 40. Joyce, M. G. *et al.* Soluble Prefusion Closed DS-SOSIP.664-Env Trimers of Diverse HIV-1
711 Strains. *Cell Rep.* **21**, 2992–3002 (2017).

712 41. Kumar, S. *et al.* B cell repertoire sequencing of HIV-1 pediatric elite-neutralizers identifies
713 multiple broadly neutralizing antibody clonotypes. *Front. Immunol.* **15**, 1272493 (2024).
714 42. Sanders, R. W. *et al.* Stabilization of the soluble, cleaved, trimeric form of the Envelope
715 glycoprotein complex of human immunodeficiency virus type 1. *J. Virol.* **76**, 8875–8889
716 (2002).
717 43. Klasse, P. J. *et al.* Influences on trimerization and aggregation of soluble, cleaved HIV-1 SOSIP
718 Envelope glycoprotein. *J. Virol.* **87**, 9873–9885 (2013).
719 44. de Taeye, S. W. *et al.* Immunogenicity of Stabilized HIV-1 Envelope Trimers with Reduced
720 Exposure of Non-neutralizing Epitopes. *Cell* **163**, 1702–1715 (2015).
721 45. Andrabi, R. *et al.* The Chimpanzee SIV Envelope Trimer: Structure and Deployment as an HIV
722 Vaccine Template. *Cell Rep.* **27**, 2426-2441.e6 (2019).
723 46. A Recombinant Human Immunodeficiency Virus Type 1 Envelope Glycoprotein Complex
724 Stabilized by an Intermolecular Disulfide Bond between the gp120 and gp41 Subunits Is an
725 Antigenic Mimic of the Trimeric Virion-Associated Structure | Journal of Virology.
726 https://journals.asm.org/doi/full/10.1128/JVI.74.2.627-643.2000.
727 47. Binley, J. M. *et al.* Enhancing the proteolytic maturation of human immunodeficiency virus
728 type 1 Envelope glycoproteins. *J. Virol.* **76**, 2606–2616 (2002).
729 48. Ringe, R. P. *et al.* Improving the Expression and Purification of Soluble, Recombinant Native-
730 Like HIV-1 Envelope Glycoprotein Trimers by Targeted Sequence Changes. *J. Virol.* **91**,
731 (2017).
732 49. The Design and Immunogenicity of an HIV-1 Clade C Pediatric Envelope Glycoprotein
733 Stabilized by Multiple Platforms. https://www.mdpi.com/2076-393X/13/2/110.
734 50. Guenaga, J. *et al.* Glycine Substitution at Helix-to-Coil Transitions Facilitates the Structural
735 Determination of a Stabilized Subtype C HIV Envelope Glycoprotein. *Immunity* **46**, 792-
736 803.e3 (2017).
737 51. Rodrigues, M. Q., Alves, P. M. & Roldão, A. Functionalizing Ferritin Nanoparticles for Vaccine
738 Development. *Pharmaceutics* **13**, 1621 (2021).
739 52. López-Sagaseta, J., Malito, E., Rappuoli, R. & Bottomley, M. J. Self-assembling protein
740 nanoparticles in the design of vaccines. *Comput. Struct. Biotechnol. J.* **14**, 58–68 (2016).
741 53. Schommers, P. *et al.* Restriction of HIV-1 Escape by a Highly Broad and Potent Neutralizing
742 Antibody. *Cell* **180**, 471-489.e22 (2020).

743 54. Julien, J.-P. *et al.* Broadly Neutralizing Antibody PGT121 Allosterically Modulates CD4 Binding
744 via Recognition of the HIV-1 gp120 V3 Base and Multiple Surrounding Glycans. *PLoS Pathog.*
745 **9**, e1003342 (2013).
746 55. Kumar, S. *et al.* A $V_H$ 1-69 antibody lineage from an infected Chinese donor potently
747 neutralizes HIV-1 by targeting the V3 glycan supersite. *Sci. Adv.* **6**, eabb1328 (2020).
748 56. Barnes, C. O. *et al.* Structural characterization of a highly-potent V3-glycan broadly
749 neutralizing antibody bound to natively-glycosylated HIV-1 Envelope. *Nat. Commun.* **9**, 1251
750 (2018).
751 57. Steichen, J. M. *et al.* A generalized HIV vaccine design strategy for priming of broadly
752 neutralizing antibody responses. *Science* **366**, eaax4380 (2019).
753 58. Saunders, K. O. *et al.* Targeted selection of HIV-specific antibody mutations by engineering B
754 cell maturation. *Science* **366**, eaay7199 (2019).
755 59. Simonich, C. A. *et al.* Kappa chain maturation helps drive rapid development of an infant HIV-
756 1 broadly neutralizing antibody lineage. *Nat. Commun.* **10**, 2190 (2019).
757 60. Guenaga, J. *et al.* Glycine Substitution at Helix-to-Coil Transitions Facilitates the Structural
758 Determination of a Stabilized Subtype C HIV Envelope Glycoprotein. *Immunity* **46**, 792-
759 803.e3 (2017).
760 61. Pancera, M. *et al.* Structure and immune recognition of trimeric pre-fusion HIV-1 Env. *Nature*
761 **514**, 455–461 (2014).
762 62. Bianchi, M. *et al.* Electron-Microscopy-Based Epitope Mapping Defines Specificities of
763 Polyclonal Antibodies Elicited during HIV-1 BG505 Envelope Trimer Immunization.
764 *Immunity* **49**, 288-300.e8 (2018).
765 63. Klasse, P. J. *et al.* Epitopes for neutralizing antibodies induced by HIV-1 Envelope
766 glycoprotein BG505 SOSIP trimers in rabbits and macaques. *PLOS Pathog.* **14**, e1006913
767 (2018).
768 64. McCoy, L. E. *et al.* Holes in the Glycan Shield of the Native HIV Envelope Are a Target of
769 Trimer-Elicited Neutralizing Antibodies. *Cell Rep.* **16**, 2327–2338 (2016).
770 65. Behrens, A.-J. *et al.* Composition and Antigenic Effects of Individual Glycan Sites of a Trimeric
771 HIV-1 Envelope Glycoprotein. *Cell Rep.* **14**, 2695–2706 (2016).
772 66. Brouwer, P. J. M. *et al.* Immunofocusing and enhancing autologous Tier-2 HIV-1
773 neutralization by displaying Env trimers on two-component protein nanoparticles. *Npj*
774 *Vaccines* **6**, 1–14 (2021).

775 67. Ozorowski, G. *et al.* Effects of Adjuvants on HIV-1 Envelope Glycoprotein SOSIP Trimers *In*
776 *Vitro. J. Virol.* **92**, (2018).
777 68. Ahmed, S. *et al.* Enhancing anti-viral neutralization response to immunization with HIV-1
778 Envelope glycoprotein immunogens. *Npj Vaccines* **8**, 1–10 (2023).
779 69. Sutar, J. *et al.* Geospatial HIV-1 subtype C gp120 sequence diversity and its predicted impact
780 on broadly neutralizing antibody sensitivity. *PLOS ONE* **16**, e0251969 (2021).
781 70. Ariën, K. K., Vanham, G. & Arts, E. J. Is HIV-1 evolving to a less virulent form in humans? *Nat.*
782 *Rev. Microbiol.* **5**, 141–151 (2007).
783 71. Taylor, B. S., Sobieszczyk, M. E., McCutchan, F. E. & Hammer, S. M. The challenge of HIV-1
784 subtype diversity. *N. Engl. J. Med.* **358**, 1590–1602 (2008).
785 72. Huang, A. *et al.* Global Comparison of Drug Resistance Mutations After First-Line
786 Antiretroviral Therapy Across Human Immunodeficiency Virus-1 Subtypes. *Open Forum*
787 *Infect. Dis.* **3**, ofv158 (2016).
788 73. Julien, J.-P. *et al.* Design and structure of two HIV-1 clade C SOSIP.664 trimers that increase
789 the arsenal of native-like Env immunogens. *Proc. Natl. Acad. Sci. U. S. A.* **112**, 11947–11952
790 (2015).
791 74. Kumar, S. *et al.* Neutralizing Antibodies Induced by First-Generation gp41-Stabilized HIV-1
792 Envelope Trimers and Nanoparticles. *mBio* **12**, 10.1128/mbio.00429-21 (2021).
793 75. Borst, A. J. *et al.* Germline VRC01 antibody recognition of a modified clade C HIV-1 Envelope
794 trimer and a glycosylated HIV-1 gp120 core. *eLife* **7**, e37688 (2018).
795 76. Ringe, R. P. *et al.* Glycan heterogeneity as a cause of the persistent fraction in HIV-1
796 neutralization. *PLOS Pathog.* **19**, e1011601 (2023).
797 77. Xu, D. *et al.* Design of universal Ebola virus vaccine candidates via immunofocusing. *Proc.*
798 *Natl. Acad. Sci. U. S. A.* **121**, e2316960121.
799 78. Powell, A. E. *et al.* Multimerization of Ebola GPΔmucin on protein nanoparticle vaccines has
800 minimal effect on elicitation of neutralizing antibodies. *Front. Immunol.* **13**, 942897 (2022).
801 79. Casazza, J. P. *et al.* Phase 1 dose-escalation trial evaluating a group 2 influenza hemagglutinin
802 stabilized stem nanoparticle vaccine. *Npj Vaccines* **9**, 1–10 (2024).
803 80. Tang, P. *et al.* A ferritin nanoparticle vaccine based on the hemagglutinin extracellular
804 domain of swine influenza A (H1N1) virus elicits protective immune responses in mice and
805 pigs. *Front. Immunol.* **15**, (2024).
806 81. Stephens, L. M. & Varga, S. M. Nanoparticle vaccines against respiratory syncytial virus.
807 *Future Virol.* **15**, 763–778.

808 82. Swanson, K. A. *et al.* A respiratory syncytial virus (RSV) F protein nanoparticle vaccine
809 focuses antibody responses to a conserved neutralization domain. *Sci. Immunol.* **5**, eaba6466
810 (2020).
811 83. Joyce, M. G. *et al.* SARS-CoV-2 ferritin nanoparticle vaccines elicit broad SARS coronavirus
812 immunogenicity. *bioRxiv* 2021.05.09.443331 (2021) doi:10.1101/2021.05.09.443331.
813 84. Weidenbacher, P. A.-B. *et al.* A ferritin-based COVID-19 nanoparticle vaccine that elicits
814 robust, durable, broad-spectrum neutralizing antisera in non-human primates. *Nat. Commun.*
815 **14**, 2149 (2023).
816 85. Yu, J. *et al.* Ad26.COV2.S and SARS-CoV-2 spike protein ferritin nanoparticle vaccine protect
817 against SARS-CoV-2 Omicron BA.5 challenge in macaques. *Cell Rep. Med.* **4**, 101018 (2023).
818 86. Johnston, S. C. *et al.* A SARS-CoV-2 Spike Ferritin Nanoparticle Vaccine Is Protective and
819 Promotes a Strong Immunological Response in the Cynomolgus Macaque Coronavirus
820 Disease 2019 (COVID-19) Model. *Vaccines* **10**, 717 (2022).
821 87. Guenaga, J. *et al.* Structure-Guided Redesign Increases the Propensity of HIV Env To Generate
822 Highly Stable Soluble Trimers. *J. Virol.* **90**, 2806–2817 (2016).
823 88. Rappuoli, R., Bottomley, M., D'Oro, U., Finco, O. & Gregorio, E. Reverse vaccinology 2.0:
824 Human immunology instructs vaccine antigen design. *J. Exp. Med.* **213**, jem.20151960 (2016).
825 89. Klasse, P. J., Ozorowski, G., Sanders, R. W. & Moore, J. P. Env Exceptionalism: Why Are HIV-1
826 Env Glycoproteins Atypical Immunogens? *Cell Host Microbe* **27**, 507–518 (2020).
827 90. Seabright, G. E., Doores, K. J., Burton, D. R. & Crispin, M. Protein and Glycan Mimicry in HIV
828 Vaccine Design. *J. Mol. Biol.* **431**, 2223–2247 (2019).
829 91. Veneziano, R. *et al.* Role of nanoscale antigen organization on B-cell activation probed using
830 DNA origami. *Nat. Nanotechnol.* **15**, 716–723 (2020).
831 92. ACTS, RULES AND GUIDELINES: Committee for the Purpose of Control And Supervision of
832 Experiments on Animals.
833 https://ccsea.gov.in/Content/54_1_ACTS,RULESANDGUIDELINES.aspx.
834 93. Sok, D. *et al.* Recombinant HIV Envelope trimer selects for quaternary-dependent antibodies
835 targeting the trimer apex. *Proc. Natl. Acad. Sci. U. S. A.* **111**, 17624–17629 (2014).
836 94. del Moral-Sánchez, I. *et al.* Triple tandem trimer immunogens for HIV-1 and influenza nucleic
837 acid-based vaccines. *Npj Vaccines* **9**, 1–18 (2024).
838 95. Kumar, S. *et al.* Recognition determinants of improved HIV-1 neutralization by a heavy chain
839 matured pediatric antibody. *iScience* **26**, 107579 (2023).

840 96. Tang, G. *et al.* EMAN2: An extensible image processing suite for electron microscopy. *J. Struct.*
841 *Biol.* **157**, 38–46 (2007).
842 97. Kumar, A., P., S., Gulati, S. & Dutta, S. User-friendly, High-throughput, and Fully Automated
843 Data Acquisition Software for Single-particle Cryo-electron Microscopy. *J. Vis. Exp.* 62832
844 (2021) doi:10.3791/62832.
845 98. Scheres, S. H. W. RELION: Implementation of a Bayesian approach to cryo-EM structure
846 determination. *J. Struct. Biol.* **180**, 519–530 (2012).
847 99. Punjani, A., Rubinstein, J. L., Fleet, D. J. & Brubaker, M. A. cryoSPARC: algorithms for rapid
848 unsupervised cryo-EM structure determination. *Nat. Methods* **14**, 290–296 (2017).
849 100. Zheng, S. Q. *et al.* MotionCor2: anisotropic correction of beam-induced motion for
850 improved cryo-electron microscopy. *Nat. Methods* **14**, 331–332 (2017).
851 101. Rohou, A. & Grigorieff, N. CTFFIND4: Fast and accurate defocus estimation from electron
852 micrographs. *J. Struct. Biol.* **192**, 216–221 (2015).
853 102. Grant, T., Rohou, A. & Grigorieff, N. cisTEM, user-friendly software for single-particle
854 image processing. *eLife* **7**, e35383 (2018).
855 103. Mishra, N. *et al.* Broadly neutralizing plasma antibodies effective against autologous
856 circulating viruses in infants with multivariant HIV-1 infection. *Nat. Commun.* **11**, 4409
857 (2020).
858 104. Montefiori, D. C. Measuring HIV Neutralization in a Luciferase Reporter Gene Assay. in *HIV*
859 *Protocols* (eds. Prasad, V. R. & Kalpana, G. V.) 395–405 (Humana Press, Totowa, NJ, 2009).
860 doi:10.1007/978-1-59745-170-3_26.
861
862 **FIGURE LEGENDS:**
863
864 **Figure 1: Design & biochemical characterization of 330 gp140 Env trimers and ferritin**
865 **nanoparticles.** Linear representation of three 330 Envelope variants **(A)** Design of SOSIP with
866 the SOS-bond (A605-T605C), IP (I559P) stabilizing mutation along with TD8 mutations, a
867 intraprotomer disulfide bond (I201C-A433C), an improved furin cleavage (R6) with CD5 Signal
868 Peptide (SP) and Twin Strep-Tag (tst) tag **(B)** Design of NFL covalently linking gp120 to gp41
869 with flexible glycine serine (GGGGSGGGGS) linker **(C)** Design of H. pylori ferritin nanoparticle
870 linked glycine serine linker to SOSIP construct **(D)** A surface structure highlighting the TD8
871 stabilizing mutations (right) in the 330 Envelope construct. Structure was illustrated using
872 PyMOL and based on the BG505 SOSIP.664 crystal structure (PDB ID: 4ZMJ) **(E)** Size-exclusion

873 chromatography (SEC) profiles of AIIMS 330 Env trimers (SOSIP and NFL) and Ferritin
874 nanoparticles (NPs), eluted between 8–12 mL on a Superdex 200 Increase 10/300 GL column **(F)**
875 Negative Stain-EM 2-D class averages of NFL & SOSIP gp140 Env trimers and ferritin
876 nanoparticles **(G)** 3D reconstruction of SOSIP gp140 Env trimers and multivalent ferritin
877 nanoparticles using chimera X **(H)** Melting curve around 74°C of AIIMS 330 Envelope

878 **Figure 2: Antigenicity of 330 gp140 Env trimers and ferritin nanoparticles to HIV-1 bNAbs**
879 **and non-NAbs.** Representative AIIMS 330 Env binding curves with conformational specific
880 bNAbs (PGT145, CAP256.25, PGDM1400, PGT151), CD4 specific bNAbs (VRC01, N6), V3
881 Supersite (10.1074, AIIMS P01) along with non-nAbs (17b+sCD4, F105, A32, 48d) assessed by
882 ELISA.

883 **Figure 3: Octet sensograms kinetics of 330 Env to HIV-1 bNAbs and non-NAbs. (B)** Octet
884 Sensograms showing response shift (nm) over time (sec) of AIIMS 330 Env trimers and particles
885 with varied concentrations (500 nM, 166.6 nM, 55.5 nM, 18.5 nM, 6.1 nM) against the quaternary
886 specific bNAbs PGT145, PGD1400, cleavage dependent bNAb PGT151 and the non-nAbs F105 &
887 17b+sCD4.

888 **Figure 4: Structural and glycan homology of 330 SOSIP with BG505 & 16055 trimers (A-B)**
889 Atomic model comparison of 330 SOSIP Env trimer with BG505 SOSIP (PDB: 4TVP) (RMSD
890 gp120: 0.685 $A^0$, gp41: 0.478 $A^0$) **(C-D)** 16055 NFL (PDB: 5UM8) (RMSD gp120: 0.798 $A^0$, gp41:
891 0.739 $A^0$) SOSIP trimer. Colour coding of SOSIP trimers corresponding to segmented EM
892 densities are: dodger blue, AIIMS 330 SOSIP, deep pink, BG505 SOSIP and 16055. Within each
893 protomer, gp120 regions are highlighted in blue and pink, while gp41 regions are shown in
894 yellow and green **(E)** Presence of glycan hole in 330 Env at position 130, 295, 339 in HXB2
895 reference coordinates showed in top, front & side view **(F)** Figure depicting the total protein
896 accessible area across cross-clade Envelopes **(G)** Presence of total 28 PNGS in AIIMS 330 &
897 BG505 Envelope. An N indicates the presence of a PNGS, if NXT/S motif in a.a sequence whereas
898 X should not be proline. The glycan structure and alignment created by N-Glycosite tool from Los
899 Alamos HIV-1 sequence database.

900 **Figure 5: Cryo-EM structure of 330 SOSIP Env trimer in complex with autologous bNAb**
901 **AIIMS 44m (A)** Top and side views of Cryo-EM reconstructed map of AIIMS 330 SOSIP Env
902 trimer in complex with 44m bNAb. Colour coding corresponding to segmented EM densities are:
903 magenta, 44m bNAb; dodger blue, gp120; gold, gp41 **(B)** The corresponding atomic model fitted

904 in the EM map of AIIMS 330 SOSIP trimer in complex with 44m bNAb. The model illustrates that
905 three 44m bNAbs bind to each gp120 monomeric subunit, facilitating effective neutralization
906 **(C)** Location of CDRH and FR3 regions are shown here in different colours (CDRH1- cyan,
907 CDRH2- deep green, CDRH3- light green, FR3- light brown) **(D)** Key interacting residues AIIMS
908 44m bNAb - H31, Y52, Y53, and R109 highlighted in cyan colour, and corresponding interacting
909 residues of gp120 loops - T144, D325, N332, and T413 highlighted in yellow colour **(E)** The N-
910 glycans N146, N301, and N332 located at the junction of AIIMS 44m bNAb and AIIMS 330 gp120
911 protomers **(F)** The D325 residue from the Env V3 loop oriented toward a hydrophobic cleft in
912 the mAb CDRH2 region.

913 **Figure 6: Immunogenicity & Neutralizing potential of 330 SOSIP, NFL Env trimers &**
914 **Ferritin NP's in NZW rabbits. (A)** Rabbit immunization Schedule. Four groups of rabbits were
915 immunized at week 0 (prime), 4 & 20 (boost), gp140 SOSIP and NFL Env immunogens (G1 and
916 G2) were administered at a dose of 20 µg of trimers, or an equivalent molar amount SOSIP-
917 ferritin nanoparticles (25 µg) (G3) formulated with the AddaVax adjuvant (1:1 v/v). Sera was
918 obtained at indicated intervals of week 4, 6, 8, 12, 16, 20 & 22 (red arrows). **(B)** Binding
919 endpoint titers (OD at A450) over time against autologous virus (330.16.E6) Dots and error bars
920 represent the median binding titers and standard deviations. The assay cut-off is marked with a
921 dotted line **(C)** Midpoint neutralization titers ($ID_{50}$) for week 22 sera of the immunized rabbits
922 against autologous (330.16.E6) and closely related (329.14.B1), and heterologous clade C
923 (MW965.26 and 25925), Tier 1 clade B (SF162), and Tier 2 clade A (BG505.T332N)
924 pseudoviruses. Median ID50 titers NFL, SOSIP & Ferritin NP group was 375, 830 & 1160.
925 Statistical analysis was done using an unpaired two-tailed Student's t-test and the assay cut-off is
926 marked with a dotted line.

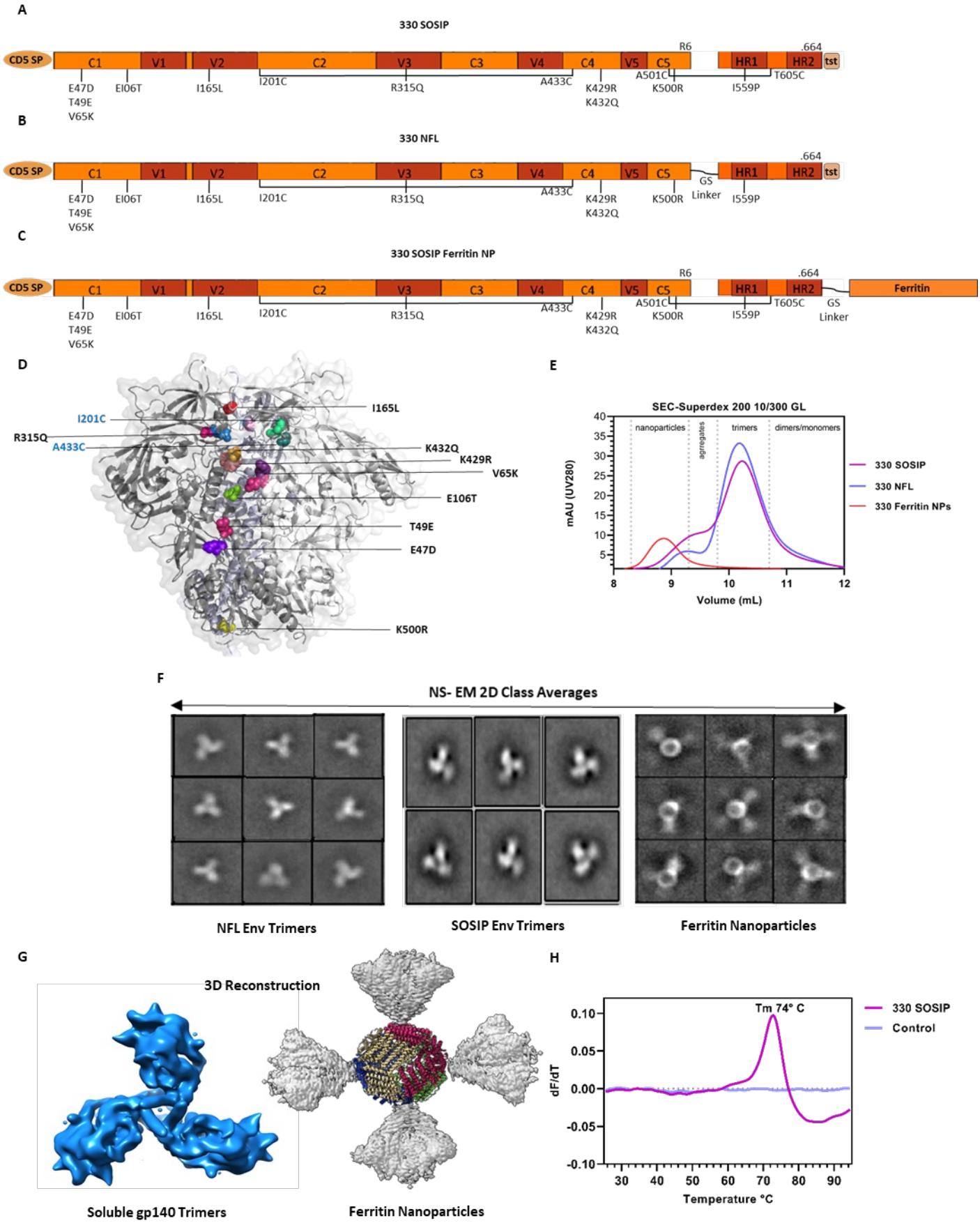
A
330 SOSIP
CD5 SP
C1
V1
V2
C2
V3
C3
V4
C4
V5
C5
R6
HR1
HR2
.664
tst
E47D
T49E
V65K
EI06T
I165L
I201C
R315Q
A433C
K429R
K432Q
A501C
K500R
I559P
T605C
B
330 NFL
GS
Linker
C
330 SOSIP Ferritin NP
Ferritin
D
I165L
I201C
R315Q
A433C
K432Q
K429R
V65K
E106T
T49E
E47D
K500R
E
SEC-Superdex 200 10/300 GL
nanoparticles
agregates
trimers
dimers/monomers
mAU (UV280)
Volume (mL)
330 SOSIP
330 NFL
330 Ferritin NPs
F
NS- EM 2D Class Averages
NFL Env Trimers
SOSIP Env Trimers
Ferritin Nanoparticles
G
3D Reconstruction
Soluble gp140 Trimers
Ferritin Nanoparticles
H
Tm 74° C
dF/dT
Temperature °C
330 SOSIP
Control

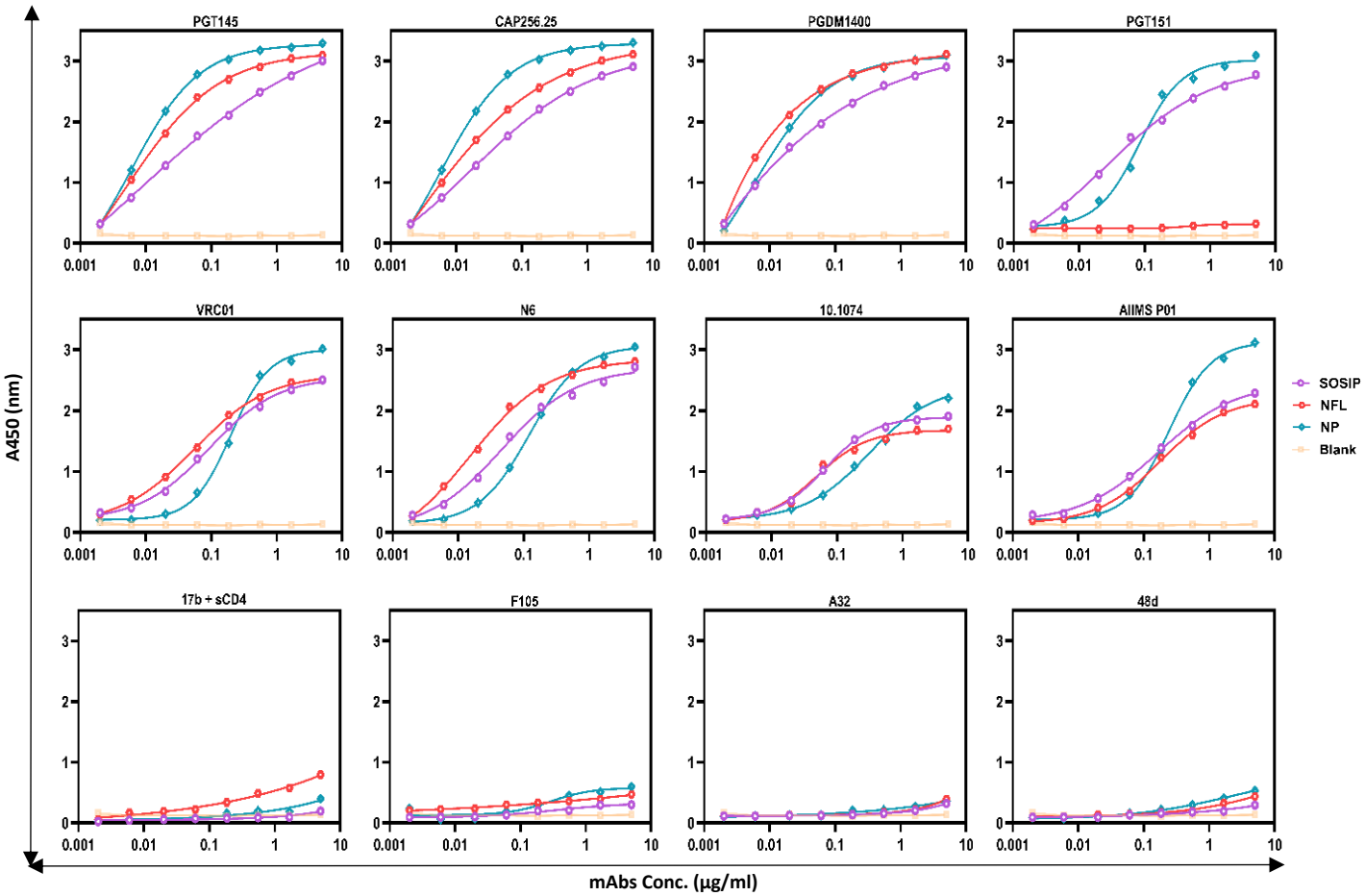
PGT145
CAP256.25
PGDM1400
PGT151
VRC01
N6
10.1074
AIIMS P01
17b + sCD4
F105
A32
48d
A450 (nm)
mAbs Conc. (µg/ml)
SOSIP
NFL
NP
Blank

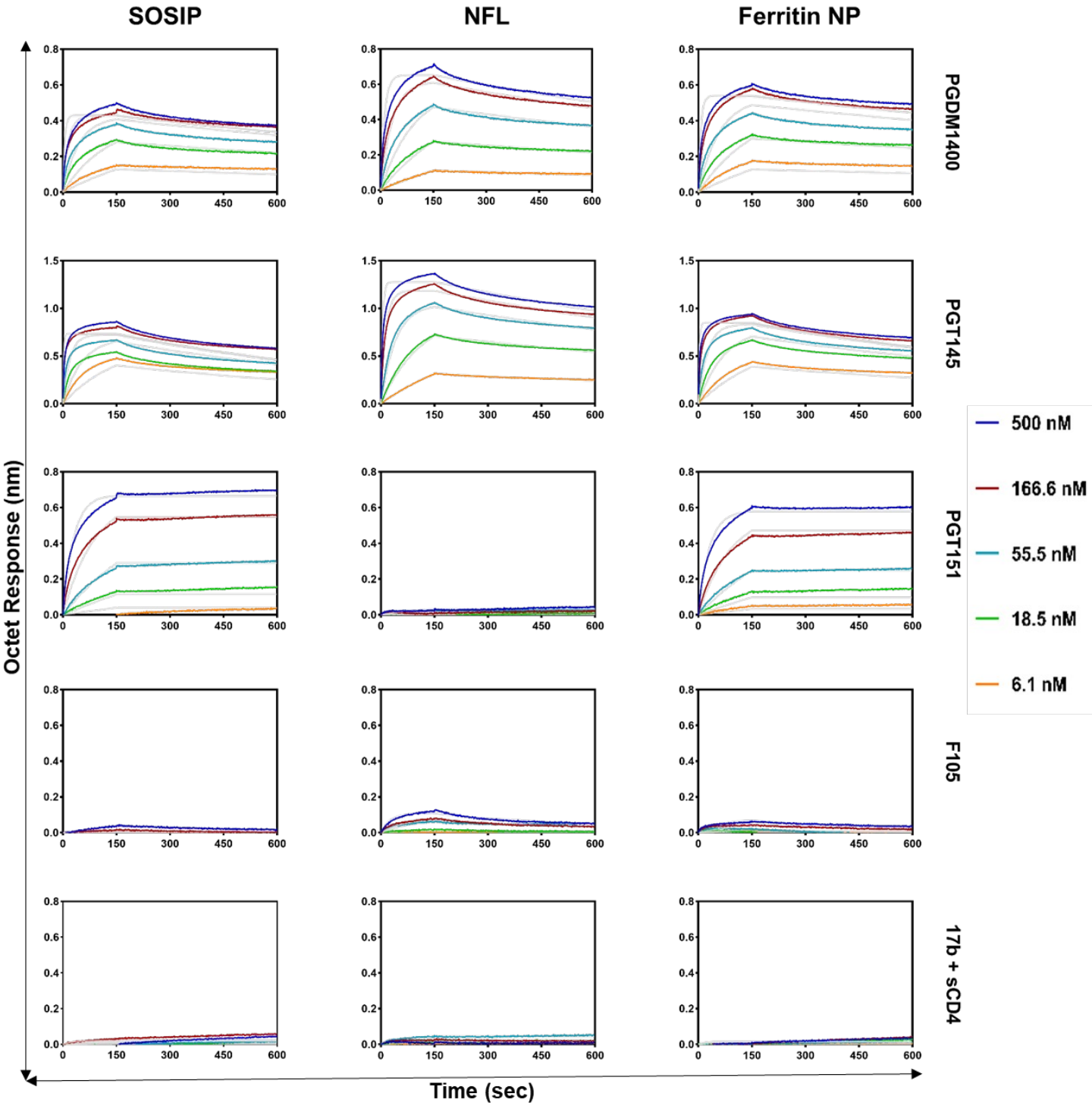
SOSIP
NFL
Ferritin NP
PGDM1400
PGT145
PGT151
F105
17b + sCD4
Octet Response (nm)
Time (sec)
500 nM
166.6 nM
55.5 nM
18.5 nM
6.1 nM

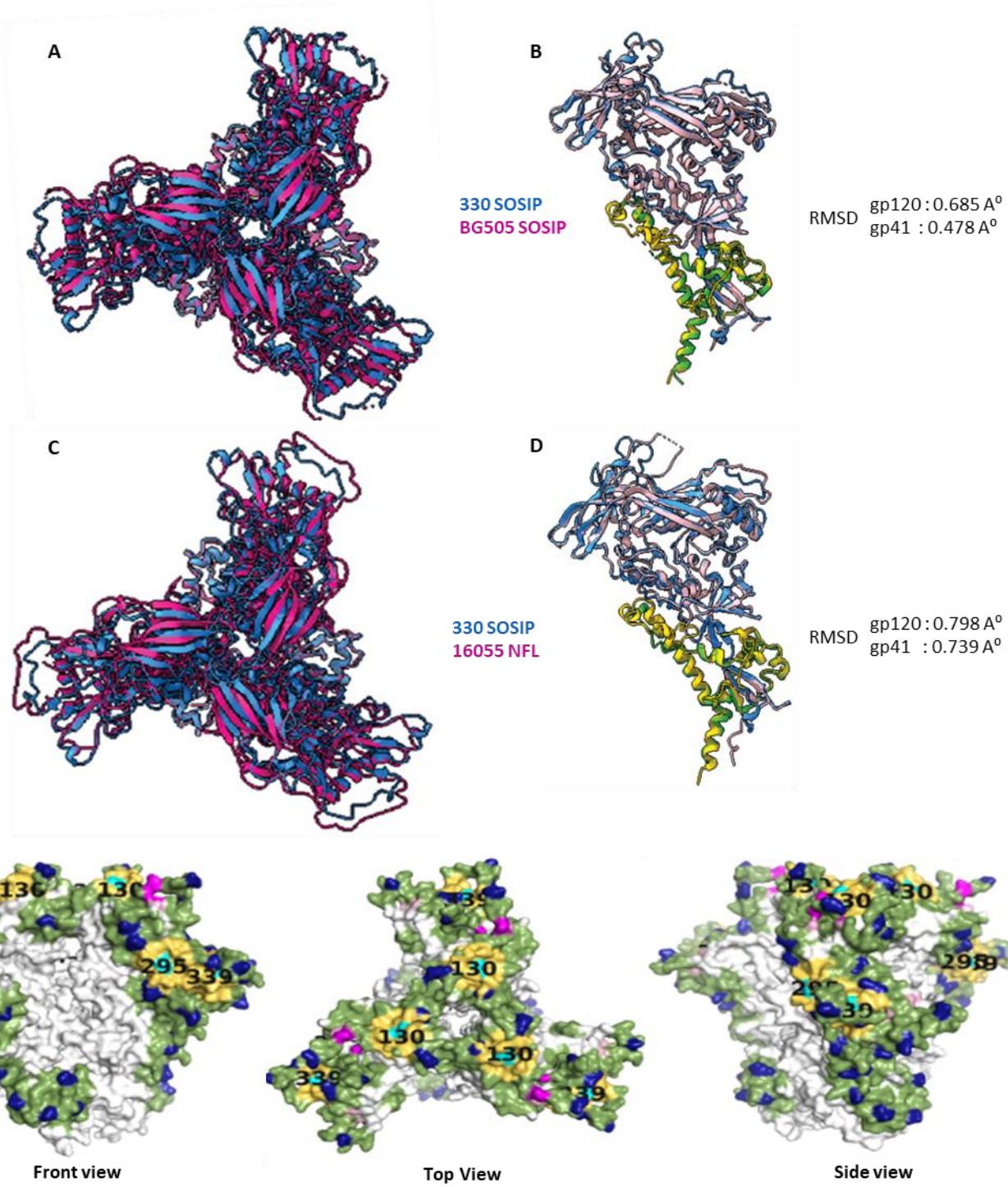
A
B
330 SOSIP
BG505 SOSIP
RMSD
gp120 : 0.685 A°
gp41 : 0.478 A°
C
D
330 SOSIP
16055 NFL
RMSD
gp120 : 0.798 A°
gp41 : 0.739 A°
E
Front view
Top View
Side view

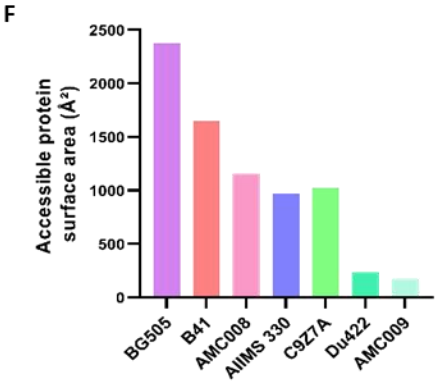
F
Accessible protein surface area (Å²)
2500
2000
1500
1000
500
0
BG505
B41
AMC008
AIIMS 330
C9Z7A
Du422
AMC009

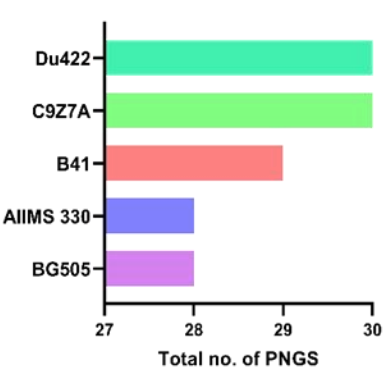
G
Du422
C9Z7A
B41
AIIMS 330
BG505
27
28
29
30
Total no. of PNGS

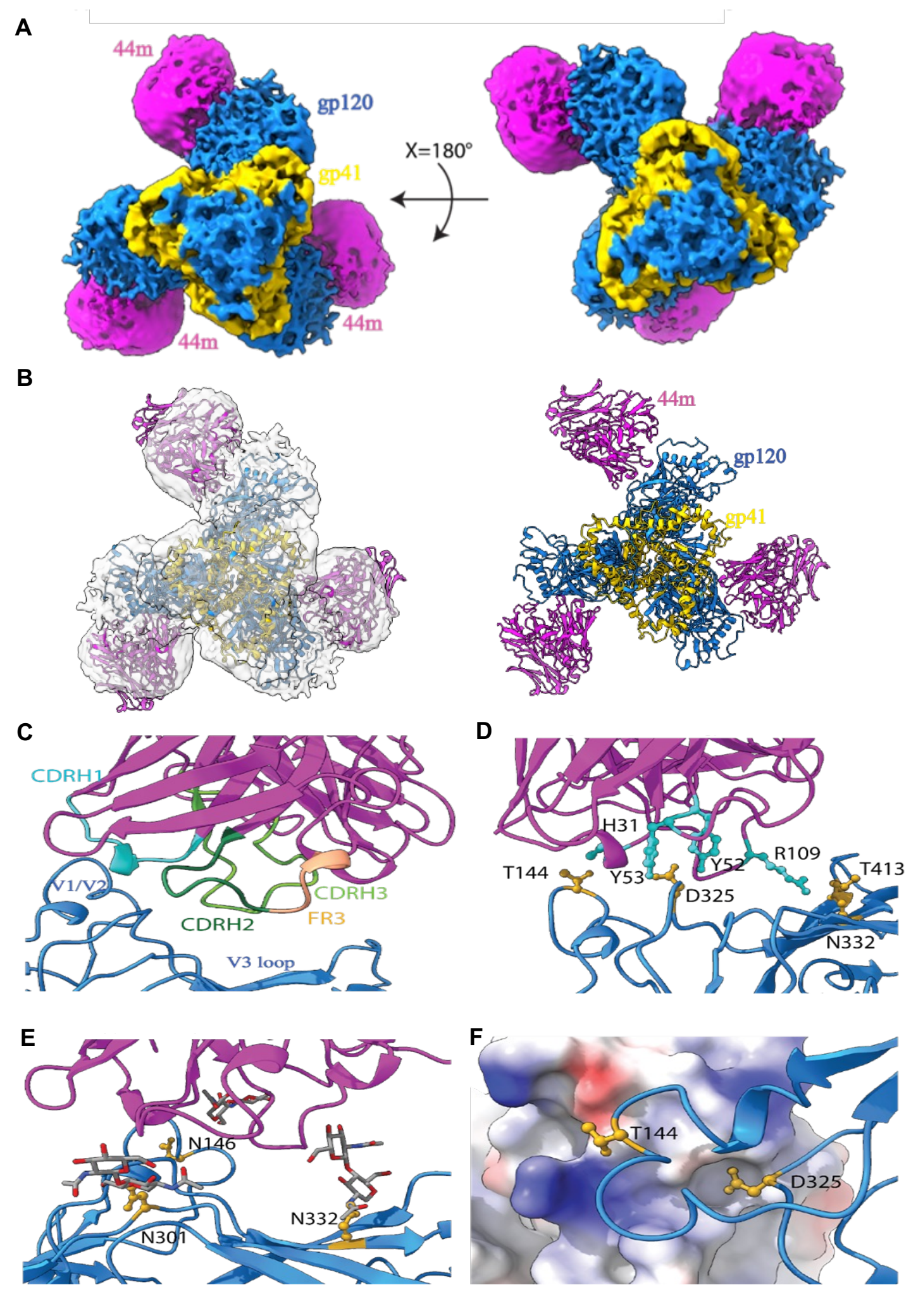
A
44m
gp120
gp41
X=180°
44m
44m
B
44m
gp120
gp41
C
CDRH1
V1/V2
CDRH3
CDRH2
FR3
V3 loop
D
H31
T144
Y53
Y52
R109
D325
T413
N332
E
N146
N332
N301
F
T144
D325

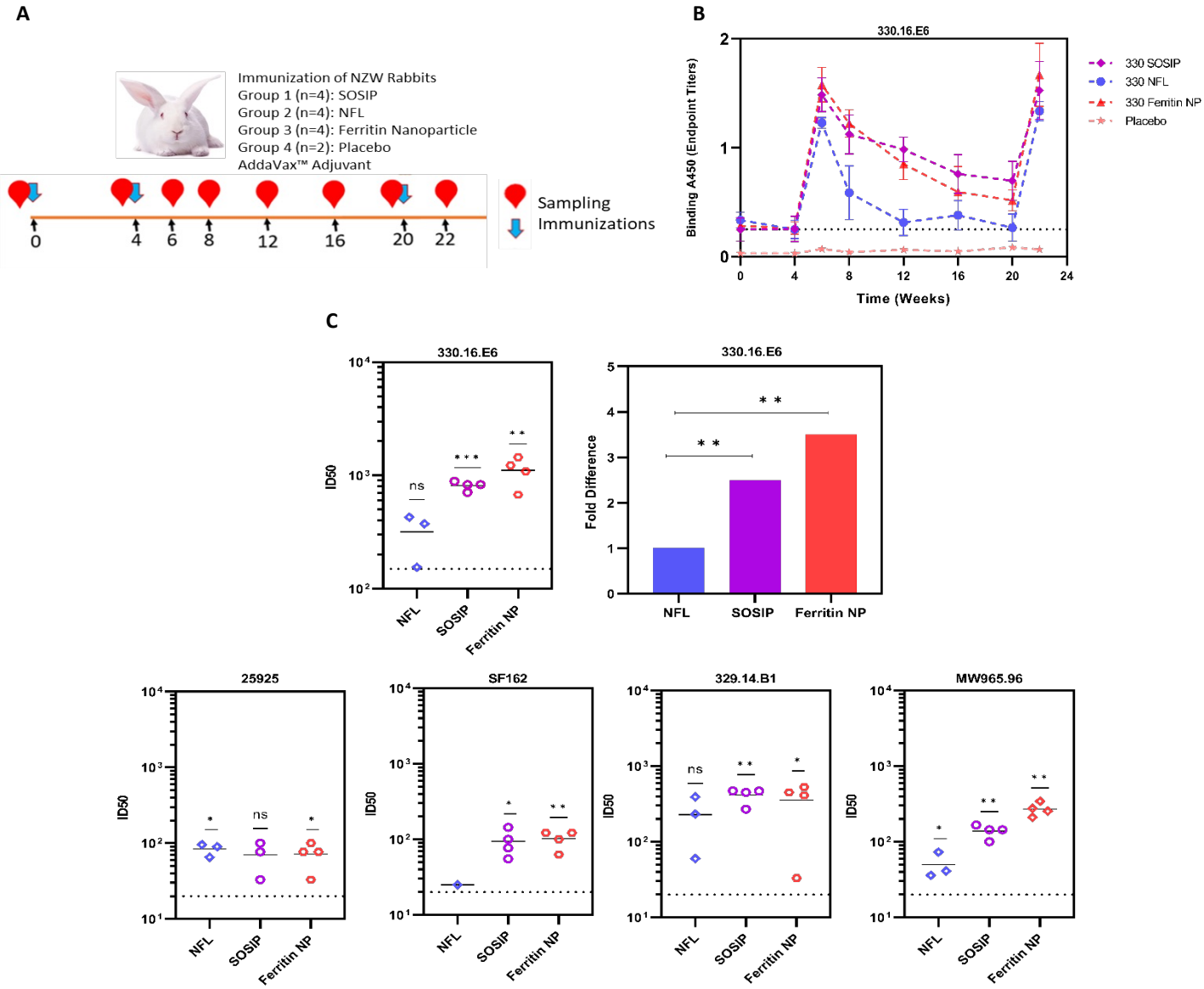
A
Immunization of NZW Rabbits
Group 1 (n=4): SOSIP
Group 2 (n=4): NFL
Group 3 (n=4): Ferritin Nanoparticle
Group 4 (n=2): Placebo
AddaVax™ Adjuvant
0
4
6
8
12
16
20
22
Sampling
Immunizations
B
330.16.E6
Binding A450 (Endpoint Titers)
Time (Weeks)
330 SOSIP
330 NFL
330 Ferritin NP
Placebo
C
330.16.E6
ID50
ns
* * *
* *
NFL
SOSIP
Ferritin NP
330.16.E6
Fold Difference
* *
* *
25925
SF162
329.14.B1
MW965.96